MATERIAL CHARACTERIZATION AND FRACTURE PREDICTION OF FDM PRINTED PARTS

by

SANCHITA SHETH

THESIS

Presented to the Faculty of the Graduate School of

The University of Texas at Arlington in Partial Fulfilment

of the Requirements

for the Degree of

MASTER OF SCIENCE IN MECHANICAL ENGINEERING

THE UNIVERSITY OF TEXAS AT ARLINGTON

DECEMBER 2019

Acknowledgements

I would like to take this opportunity to express my sincere gratitude and thanks to all who have supported me with my work and would like to acknowledge their role in it. Dr. Robert Taylor has been a mentor with his constant guidance and motivation for this work. Dr. Endel Iarve and Dr. Hari Kishore Adluru have supported with providing access to UTARI (The University of Texas at Arlington Research Institute) and their guidance with BSAM software.

Tensile and Fracture testing has been conducted with support from Dr. Ashfaq Adnan's lab. Mr. Hassan provided with the necessary training to conduct the tests. Static tensile test data referenced in Section A was generated under contract to Stratasys, Inc. in support of America Makes Design Guidance for Additive Manufacturing, Fall 2016.

The heating fixture for the fracture specimens was manufactured with training and guidance from Rex Winfrey. Manjarik Mrinal, from Dr. Cheng Luo's lab provided access to the oven and microscope for images.

Abstract

In order to take advantage of the design freedom that Additive Manufacturing offers, most applications require reliable material characterization. This can ensure that a design performs within its environment and life requirements. This work discusses two models. One investigates the raster angle dependency of stiffness properties and the other numerically predicts fracture in Fused Deposition Modeling (FDM) printed polymer parts. Pre-processing of FDM geometry was done in Abaqus CAE (SIMULIA^{TM}). FEA and post-processing was done in BSAM, which is a damage prediction software developed for composites. BSAM uses a regularized extended finite element approach of Discrete Damage Modeling. In BSAM, boundary conditions, connectivity and material properties have been specified. A similar trend in the stiffness properties was observed when the predicted modulus values were compared to experimental test data. FDM printed DCB specimens were tested and the Mode I fracture toughness values (G_{IC}) were obtained. A set of experiments was performed to study the effect of time and temperature on the Mode I fracture toughness (G_{IC}) of ABS. The G_{IC} values can be used to develop the fracture model in BSAM. Tensile tests were performed on ABS specimens to calculate the Elastic modulus. The experimental modulus values were compared to the values obtained from the model for validation. This model provides a basis for strength and fracture prediction of FDM printed parts.

Contents

List of Figures

List of Tables

Chapter 1: Introduction

Additive Manufacturing (AM), popularly known as 3D printing is defined as the process of joining materials to make parts from 3D model data, usually layer upon layer [1]. Compared to traditional manufacturing methods that often require material removal or subtraction by one or more operations like turning, cutting, milling, drilling, shaping or other means, AM adds material. One of the greatest benefits of AM is that it can produce parts with a wide range of shapes and a high degree of complexity. Design concepts, once impossible for conventional manufacturing to achieve are now being realized, all thanks to AM's design flexibility. It unleashes the designer's creative potential, allowing them to work free of constraints.

Fused Deposition Modeling (FDM) is one of the most popular processes for polymer part printing. However, it creates parts with numerous discontinuities, stress singularities and fracture interfaces which results in anisotropic mechanical properties and a severely degraded fatigue life. The degree of severity depends on the local geometry which heavily depends on process parameters. AM's design freedom is continuously being explored and is currently being realized in a variety of lightly loaded, non-critical applications. Critical applications, such as those in the aerospace industry require reliable material characterization to ensure that parts perform within their design environment and life requirements.

This work is a step towards characterizing and predicting the mechanical behaviour of FDM parts. It comprises of two sections. The first section examines the raster angle effects on stiffness and compares results predicted by a computational model to an experimental investigation of raster orientation on stiffness [2]. The work builds on previous work by

Osborn, et al, that examined anisotropic mechanical properties of individual FDM layers using classical laminated plate theory and homogenization techniques [3][2]. The second section discusses a model developed to numerically predict fracture in FDM parts. The Mode I fracture toughness values (G_{IC}) for ABS were obtained testing Double Cantilever Beam (DCB) specimens and these values were used in the numerical model. Further, the effect of temperature and heating time on the Mode I fracture toughness values (G_{IC}) for ABS was experimentally examined.

Chapter 2: Background

2.1 Fused Deposition Modeling

In the FDM process, a flexible filament is heated to a glassy state and extruded through a controlled deposition head onto a build plate in order to build the part layer by layer vertically. For instance, in Figure 1, a filament **a)** of plastic material is fed through a heated moving head **b)** that melts and extrudes it depositing it, layer after layer, in the desired shape **c)**. A moving platform **e)** lowers after each layer is deposited. For this kind of technology additional vertical support structures **d)** are needed to sustain overhanging parts [4].

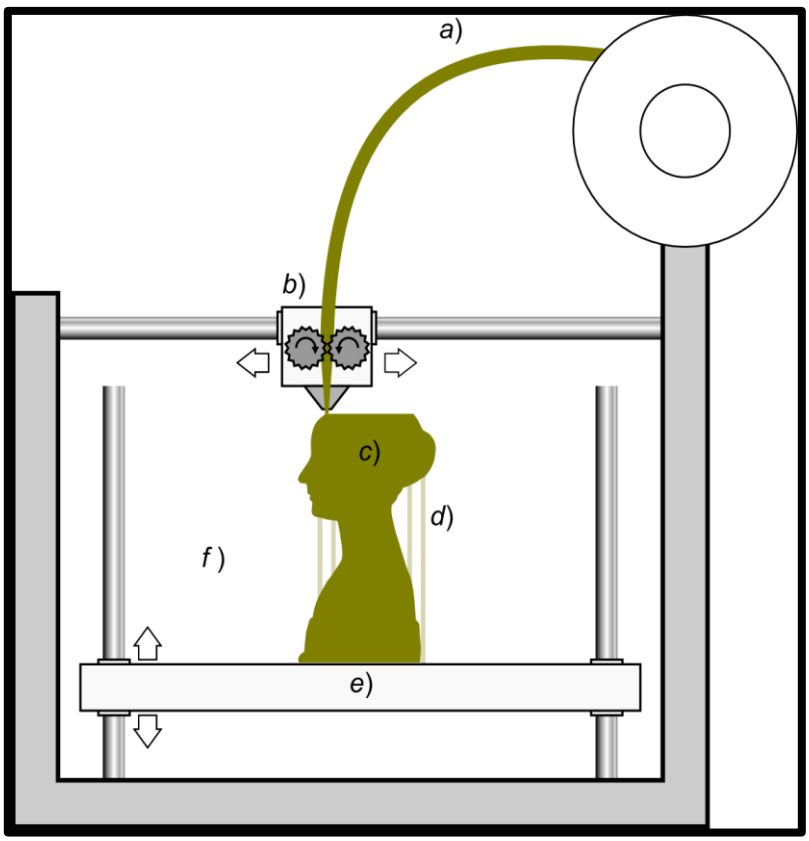

Figure 1: Schematic representation of the 3D printing technique known as FDM

Within a layer, cross-sectional geometry is deposited first in one or more contour beads to define boundaries and then an infill, which may be a solid raster or a porous pattern.

Material continuity within a part is developed as contour beads are deposited in adjacent roads and bonding takes place via diffusion welding. Part stiffness and strength therefore is a strong function of the developed inter-bead bond strength, contact area, gaps and voids as well as bead shape and orientation with respect to loading direction. These dependencies lead to anisotropic mechanical behavior within materials and parts built using FDM.

This anisotropic mechanical behavior of FDM printed materials has received significant attention in recent years and work has been performed to address the effects of FDM build parameters on stiffness, strength, fatigue, fracture, and creep. Much of the basic tensile testing follows standards like the ASTM D638 test method for tensile properties of plastics and examines process parameter effects on the resulting properties [5]. Ahn et al examined raster orientation, air gap, bead width, color, and model temperature effects on tensile and compressive strengths of directionally fabricated specimens [6]. Bellini and Guceri developed an anisotropic FDM stiffness matrix from filament testing [7]. Riddick et al executed tensile testing to study the effect of process-induced anisotropy on the mechanical response [8]. Ziemian et al executed tension, compression, 3-point bend, and tension-tension fatigue testing to characterize the anisotropic mechanical properties of ABS FDM parts, showing a strong sensitivity to raster angle and quantity of air gaps between rasters [9]. They performed further investigations and noted tensile behavior is improved by aligning the fibers of unidirectional laminae more closely with the axis of the applied stress and tensile and fatigue performance improved with alternating laminae θ°/(θ-90°) [10]. Lee and Huang performed experimental fatigue investigation on FDM ABS as a function of build orientation [11]. Afrose et al performed a similar investigation of build orientation effect on fatigue behavior of FDM PLA [12]. Zhang executed tension, creep, and fatigue testing and laminate-based finite element modeling to study mechanical property sensitivity to build orientation

[13]. Motaparti executed flexural and compression testing of ULTEM 9085 to study the individual and combined effects of build direction, raster angle, and air gap (sparse infill) build parameters on flexural and compressive stiffness and strength properties [14]. Torrado and Roberson examined tensile specimen failure and evaluated anisotropy versus geometry and raster pattern[15]. Huang and Singamneni applied experimental and analytical models of raster angle effects on modulus and strength in FDM parts [16]. Rezayat et al, developed finite element models at multiple length scales and compared results with experimental full field strain data for different raster angles and filament gaps [17]. Patel et al performed experimental investigation of fracture of FDM printed ABS for different crack length and layer of orientations [18].

Some researchers have developed methods to optimize mechanical properties. Ulu, et al developed an optimization method to enhance structural performance through build orientation optimization that recognizes these mechanical property sensitivities [19]. Torres et al likewise developed an approach for optimizing FDM part mechanical properties based on experimentally determined sensitivities to build parameters, which included layer thickness, density or infill percentage, extrusion temperature, speed, infill direction and component orientation [20].

Many researchers have shown, and validated applications of laminated plate theory used in composite materials to describe mechanical behavior in FDM printed materials. El-Gizawy, et al studied process-induced properties of FDM printed ULTEM 9085 using classical laminated plate theory to determine the anisotropic stiffness matrix and thereby establish constitutive relationships that predict the internal structure of FDM materials [21]. The authors validated the approach with tensile testing and finite element correlation. Li et al

performed theoretical and experimental analyses of mechanical properties of FDM processes and prototypes to develop constitutive models and equations to determine the elastic constants of FDM printed materials [22]. Sayre modeled FDM printed materials as a layered composite with modified properties to account for imperfect bonding between layers [23]. Rodriguez et al, obtained effective elastic moduli using a strength of materials and elasticity approach based on the asymptotic theory of homogenization and experimentally validated predicted properties [24].

Finally, much work has been performed to characterize mechanical property degradation due to FDM process characteristics. Park and Rosen addressed mechanical property degradation in cellular materials due to bounding surface errors using as-fabricated voxel modeling and a discrete homogenization approach [25]. Baikerikar examined mechanical properties for a variety of infill patterns, comparing finite element simulations and experimental results for tensile dogbone specimens [26]. Faes et al executed testing to study the influence of interlayer cooling time, which affects the coalescence of the interconnection between adjacent tracks and layers, on quasi-static properties [27].

2.2 FEM Using BSAM

BSAM is a computational structural analysis software tool developed by University of Dayton Research Institute in collaboration with the Air Force Research Laboratory, WPAFB, OH and NASA Langley Research Center, Hampton, VA [28]. It was initially developed to provide accurate stresses analysis in multilayered composite materials and further expanded for progressive failure analysis under static and fatigue loading. Discrete Damage Modelling (DDM) based on Regularized eXtended Finite Element Method (Rx-FEM) was developed for this purpose [29] [30] [31][32][33].

2.3 Discrete Damage Modeling (DDM)

A simplified damage progression sequence is shown in Figure 2(b)–(d) for the case of a laminated plate subjected to a tensile load. The stages shown are (a) initial stage ; (b) matrix cracking stage; (c) delamination stage, and (d) specimen fracture.**Error! Reference source not found.**

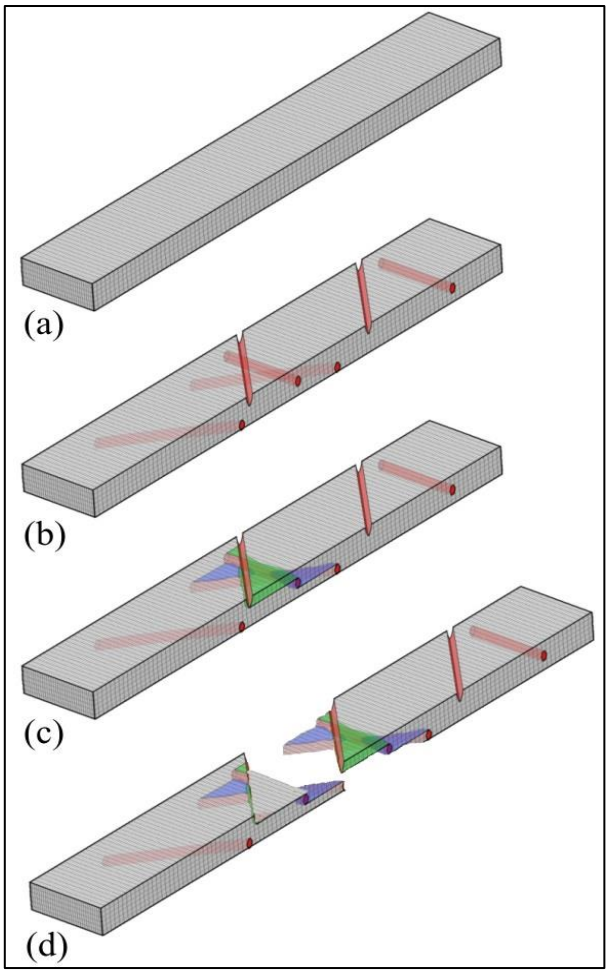

Figure 2: Idealized damage progression sequence in a laminated composite plate subjected to tensile loading.**Error! Reference source not found.**

Discrete Damage Modeling (DDM) methods are progressive failure analysis methods. DDM explicitly models displacement discontinuities associated with multiple damage events such as matrix cracking and delamination. DDM can capture multiplicity and interaction of various

failure modes. Regularized X-FEM is an implementation of DDM and is based on Traditional X-FEM.

2.4 Regularized X-FEM

In traditional X-FEM, a crack is represented by Heaviside step function. Duplicate nodes are created, and the element is split. This changes the Integration scheme. In regularized XFEM, the Heaviside function is replaced by a continuous function at the crack location. It uses the same shape functions. Duplicate elements are created which preserve the initial integration scheme [34][35].

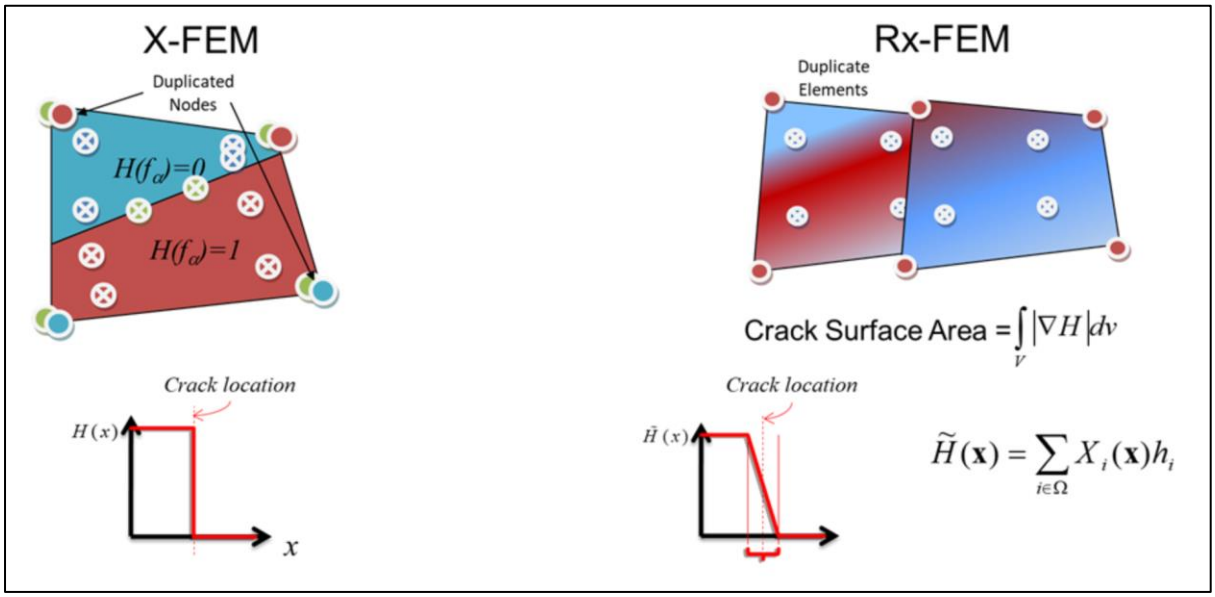

Figure 3: X-FEM vs Rx-FEM

Chapter 3: Methodology

3.1 Material Characterization

This section gives an outline of the steps involved in the Material Characterization process as shown in Figure 4. In this section, the Elastic modulus of ABS specimens were predicted using a damage prediction software called BSAM and then compared to experimental test data to verify the prediction. The process involves – (i) Modeling the FDM raster pattern in Abaqus, (ii) Meshing the specimens, (iii) Importing the specimens to BSAM, (iv) BSAM Analysis, and (v) Comparing to experimental test data.

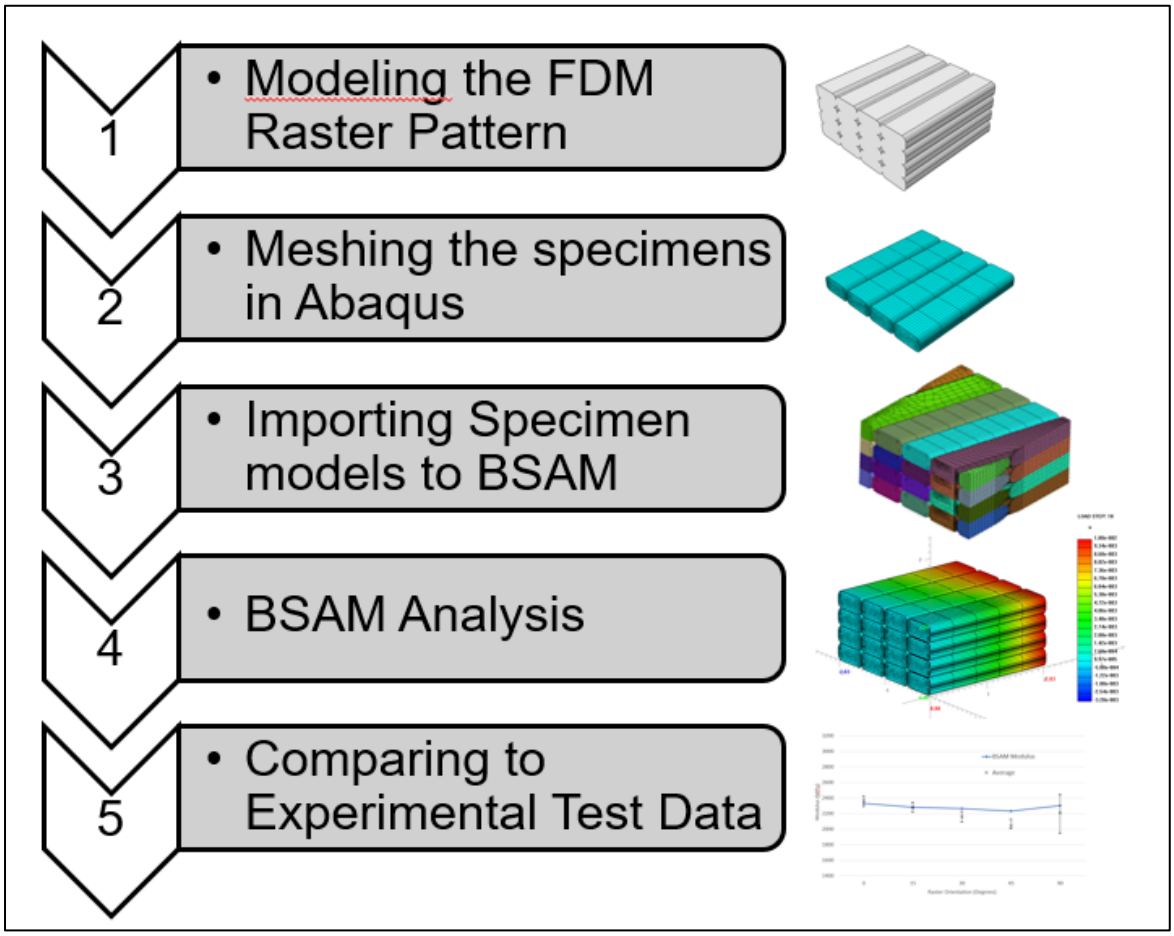

Figure 4: Overview of the Material Characterization Process

3.1.1 Modeling the FDM Raster Pattern

It was necessary to develop a model of the FDM printed geometry so that it reflects the actual nature of the part when the analysis is run.

90-degree ABS specimens were FDM printed on a Polyprinter using Simplify 3D software. These specimens were cut normal to the raster orientation and cross-sectional photographs were obtained as shown in Figure 5.

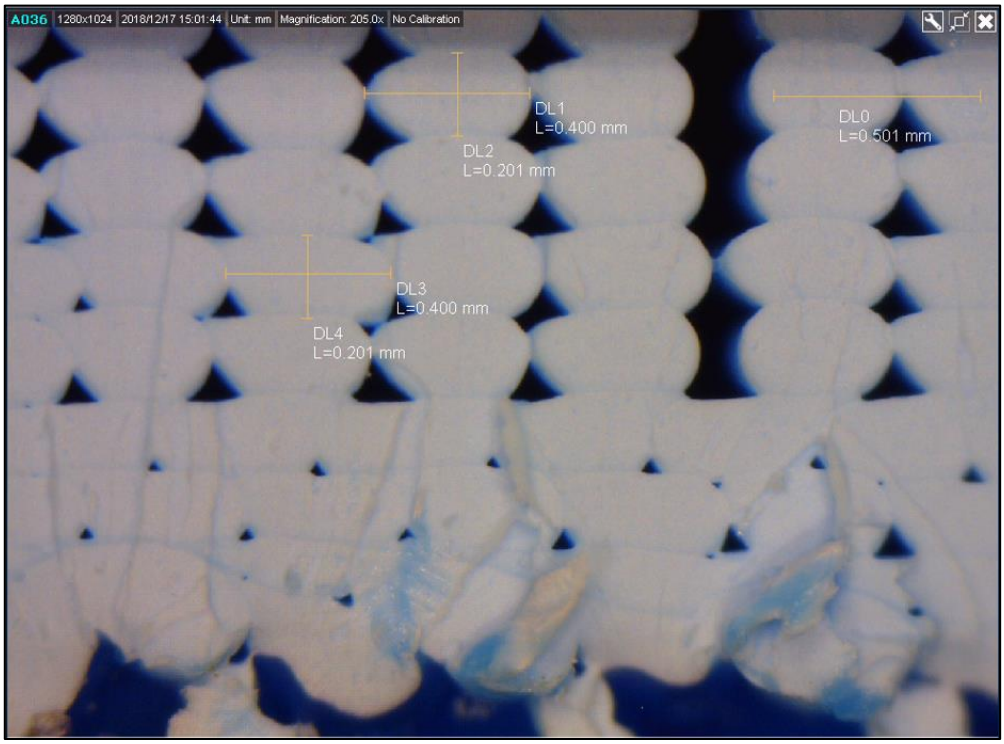

Figure 5: Image of FDM printed cross section

The cross-sectional dimensions of the specimen were obtained from this photograph and were used to create the FDM bead geometry using Abaqus as shown in Figure 6.

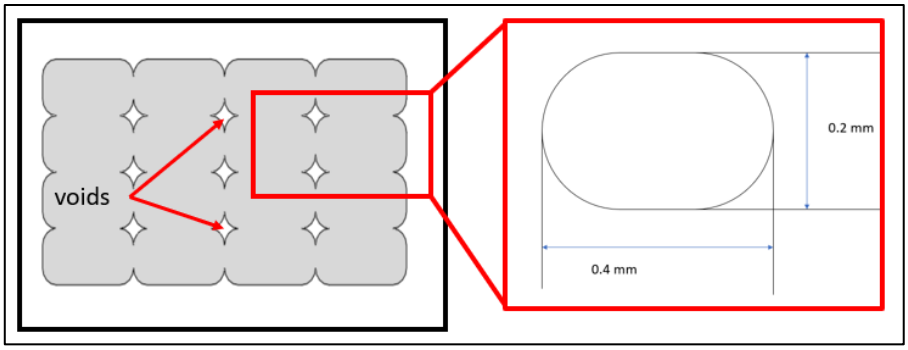

Figure 6: Cross section geometry of specimen modelled in Abaqus

3.1.2 Representative Volume Cell (RVC)

A Representative Volume Cell (RVC) was built using Abaqus/CAE 2016 based on the cross-section images. As shown in Figure 7, for the 0^o raster orientation, this volume consisted of 4 layers of roads. Each layer consisted of 4 roads. The RVC chosen is more than that required for stiffness property computation and is considered for future predictions of both failure and fracture strengths.

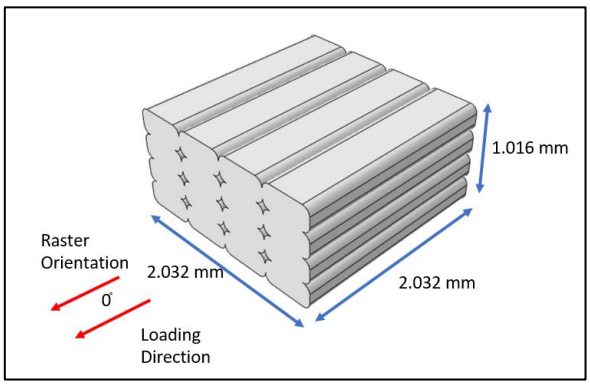

Figure 7: 0^o Representative volume cell

RVCs of the same dimensions were built for different raster orientations such as 15^o, 30^o, 45^o and 90^o as shown in Figure 8.

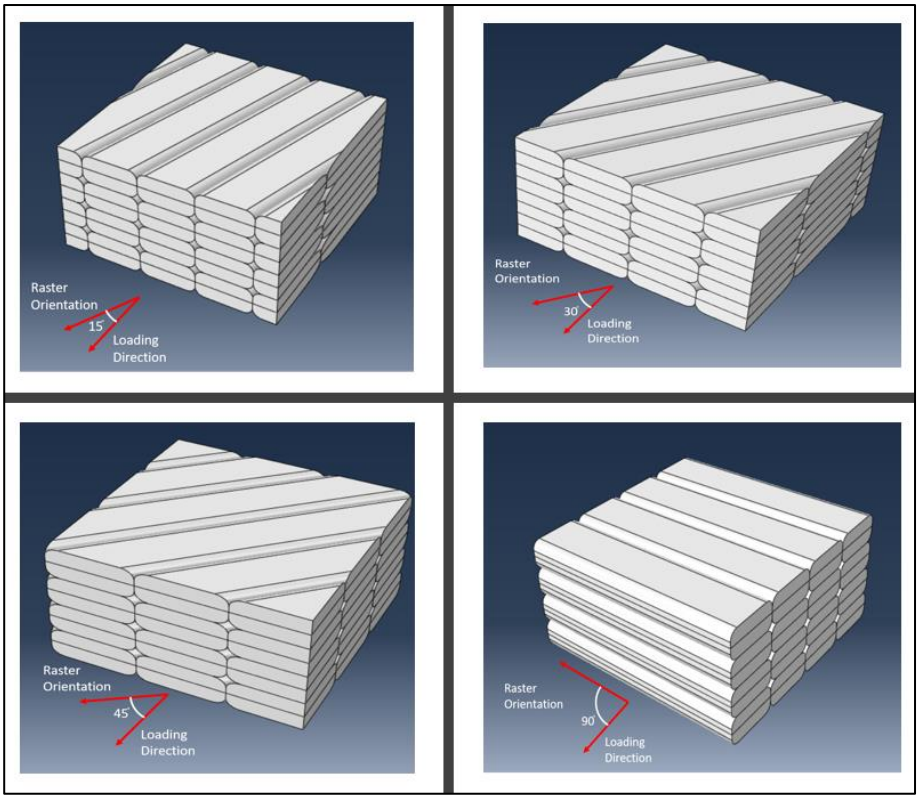

Figure 8: RVCs for other raster orientations

3.1.3 Meshing the specimens in Abaqus CAE

The bead geometry was then meshed in Abaqus as shown in Figure 9. Faces of the geometry were defined in the mesh. These faces would then be used to apply loads or identify them interfaces. An input file was generated from this mesh to be imported into the BSAM Export Module.

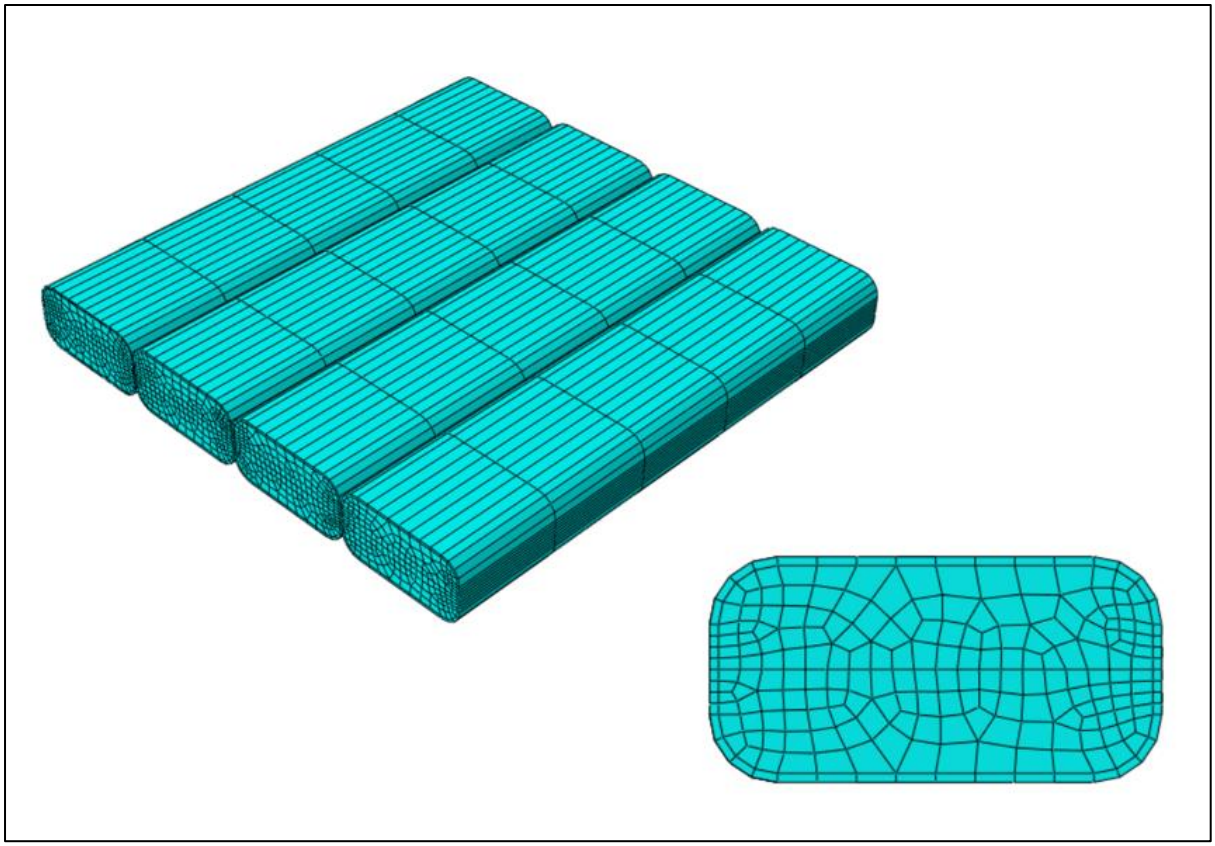

Figure 9: Meshed geometry in Abaqus

3.1.4 Importing Specimen meshes to BSAM

The Abaqus generated input file for the mesh was then imported into the BSAM export module. Here the displacement boundary condition is applied along 1-1 direction (x axis), which represent the tensile loading on the RVC. Figure 10 shows how the meshes for various raster orientations look like when imported in BSAM. It also shows how the various orientations were loaded.

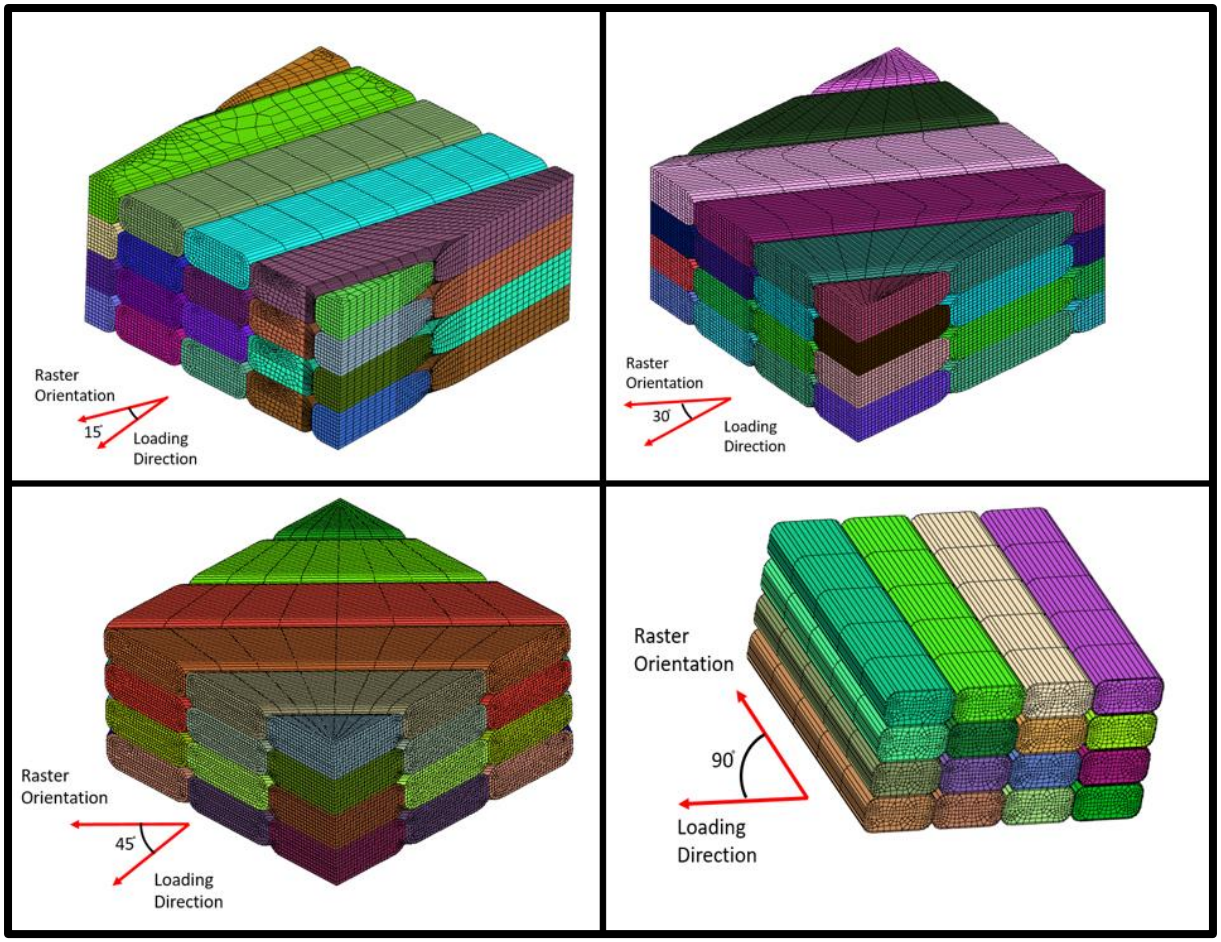

Figure 10: Various raster orientation meshes imported to BSAMs

A material file is imported to BSAM that lets one specify the properties of the material. The material used for this analysis was ULTEM9085. Bulk properties of the material were specified. Since BSAM is developed for composites, it also lets one specify the interface properties of the material. Figure 11 shows the material file that was used for analysis. It specifies properties for ULTEM9085.

```
#VTMS
*MATERIAL:  2
1               ULTEM9085       unit=SI<MM>
    2200    71.60   104 E11 Xt  Xc
    2200    71.60   104 E22 Yt  Yc
    2200            E33
    0.4 1.7 1.75    1.75    Nu13    G1c G11c    G111c
    0.4             Nu23
    0.4             Nu12
    750         G13
    750         G23
    750 57  57  G12 S   S13
    0.00134             Density
    6.527E-05           Alpha11
    6.527E-05           Alpha22
    *S-N exponent
    0   0   0   S1,S2,etta

12              StrongInterface     unit=SI<MM>
    1e+10   1.e-7           penalty displacement tolerance
    1e+8    1e+8    1e+8        Yt  Yc  S
    1.0 1.0         G1c G11c
    *Paris Law M,C
    0   0   0   0   C1,M1,C2,M2
    0               etta
    *S-N exponent
    0   0   0   S1,S2,etta

END MATERIAL
```

Figure 11: The material file for ULTEM9085

3.1.5 BSAM Analysis

The displacement on the external boundary is given by

$$u_i = \overline{\varepsilon}_{ij}\, x_j \tag{3}$$

where $\overline{\varepsilon}_{ij}$ is observer strain, which in the present case is not equal to the volume average strain due to presence of voids. Therefore, instead of direct computation of average strain, the observer strain is used. In all cases these strain values are incremented uniformly to a maximum value of 0.01. The above equation is used to assign displacement boundary conditions for all the raster orientations. The volume average stress is given by

$$\overline{\sigma}_i = \frac{1}{V}\int_V \sigma_i \, dV \tag{4}$$

The homogenized compliance matrix is computed as

$$\overline{S_i} \;=\; [\overline{\sigma_i}]^{-1}\overline{\varepsilon_i} \tag{5}$$

followed by calculation of Young's moduli using standard formulae.

3.1.6 Scope

The scope of current work is limited to determining elastic moduli, which is based on homogenization approach [36]. The homogenization method implemented in BSAM is tailored to resolve field behavior across regions where there is abrupt variation in the local microgeometry. The numerical method developed in BSAM is a fast way to extract local field information inside prescribed subdomains without having to resort to a full numerical simulation. The homogenized method used for local field assessment is explained in detail by Breitzman et al [36]. Even though the authors discussed the homogenization formulas for prestressed and/or thermomechanical loads, they can be simplified for a composite body having no initial stress.

Let a composite body be subjected to an external force f. Let uε and σε be the displacements and stresses associated with this force. Based on the homogenization procedure the asymptotic expansions for displacements uε and stresses σijε are

$$\boldsymbol{u}^{\varepsilon} \;=\; \boldsymbol{u}^{(0)}(\boldsymbol{X}) + \varepsilon\boldsymbol{u}^{(1)}(\boldsymbol{X},\boldsymbol{Y}) + \cdots \tag{1}$$

$$\;=\; \boldsymbol{u}^{(0)}(\boldsymbol{X}) + \sum_{k=1}^{\infty}\varepsilon^{k}\boldsymbol{u}^{(k)}(\boldsymbol{X},\boldsymbol{Y}) \tag{1}$$

$$\sigma_{ij}^{\varepsilon} = \sum_{k=0}^{\infty} \varepsilon^k \, \sigma_{ij}^{(k)}(\boldsymbol{X}, \boldsymbol{Y}) \qquad (2)$$

Here X are 'slow' variables, and Y = X/ε are the 'fast' variables and ε- is the characteristic size of the microstructure. Here the functions on the right side are assumed to be periodic in Y within the periodicity cell. The differential operators are represented in the form of sum of operators in X and Y by using the two-scale expansion shown in equations (1) & (2) above.

The current FDM specimens are distinguished by the presence of local periodic microstructure. In order to capture this local material heterogeneity, some form of local enhancement of approximation space is required to accurately estimate the sub structural (ply level) units.

3.1.7 Comparing with Experimental test data

To determine stiffness properties, in the BSAM export module, static displacement boundary conditions were applied to the RVC. One face of the RVC was fixed in x, y and z and on the opposite face, a displacement boundary condition of 0.1 mm was applied in slow increments. The application of the displacement boundary condition was done in steps of 1% of the total load. Next, the material file was imported into the BSAM export module. The model was then exported as a BSAM input file. The file was run in the BSAM software and outputs for displacement, force, stress and strain were generated at each step. The stiffness of the RVC was calculated from the stress and strain values.

3.2 Fracture Prediction

This section gives an outline of the Fracture Prediction process as shown in Figure 12 . An important step in fracture prediction is finding the Mode I fracture toughness value (G_{IC}) for a given material. ASTM standard D5528-13 test method describes the determination of the opening Mode I interlaminar fracture toughness (G_{IC}) of continuous fiber-reinforced composite materials using the double cantilever beam (DCB) specimen as in [37]. Since FDM printed parts are comparable to composite parts, as FDM parts are layer based, this test method was used to obtain the Mode I fracture toughness values (G_{IC}) for FDM printed DCB specimens of ABS material.

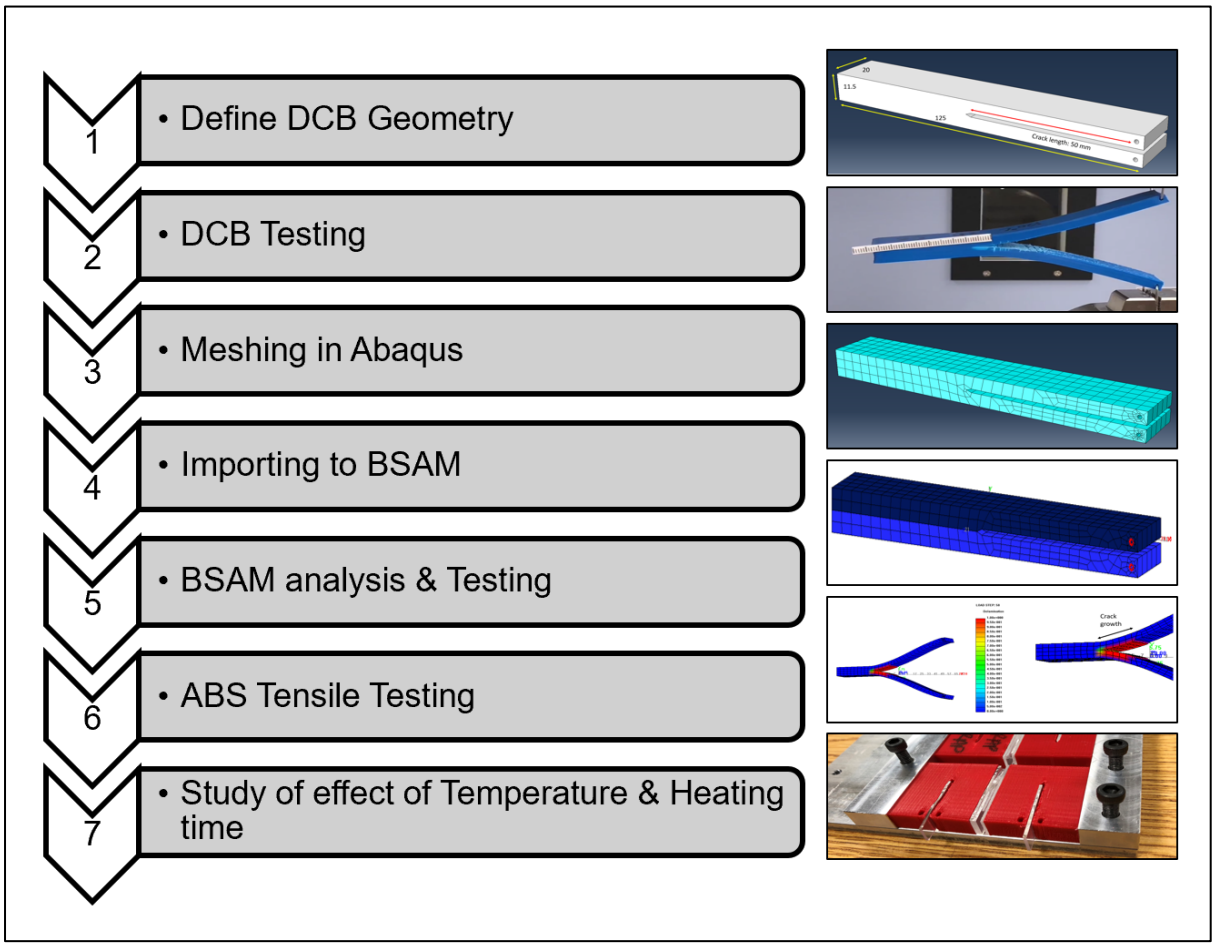

Figure 12: Overview of Fracture Prediction Process

3.2.1 Define DCB Geometry

According to ASTM D5528, the DCB specimen geometry shall be at least 125 mm (5.0 in.) long and nominally from 20 to 25 mm (0.8 to 1.0 in.) wide, inclusive. The thickness shall normally be between 3 to 5 mm (0.12 to 0.2 in.) and the initial delamination length measured from the load line to the end of the insert, shall normally be 50 mm. Also, a/h (<10) is not recommended [37]. Figure 13 is an example specimen from ASTM D5528.

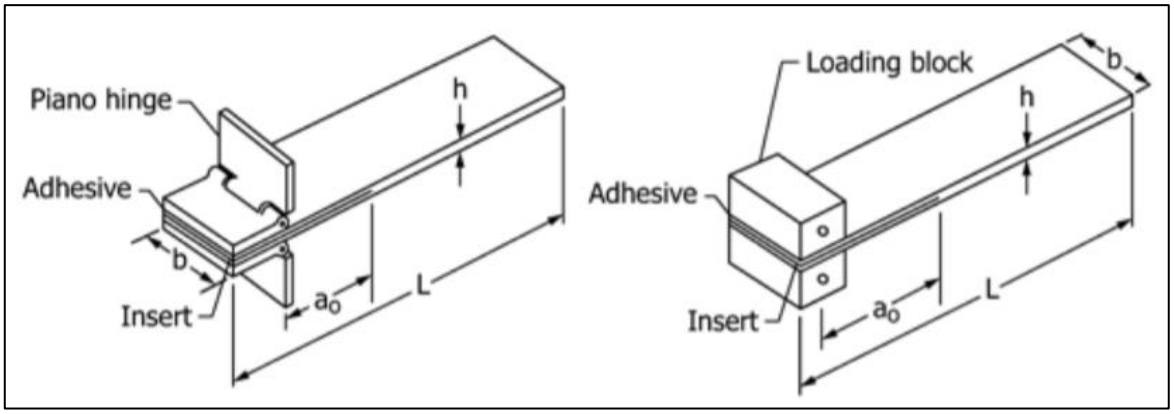

Figure 13: DCB Specimen in ASTM D5528

Accordingly, the DCB specimen was modelled in Abaqus as shown in Figure 14. The thickness was increased to integrate the loading block into the specimen. It also ensures that there is sufficient amount of FDM printed layers.

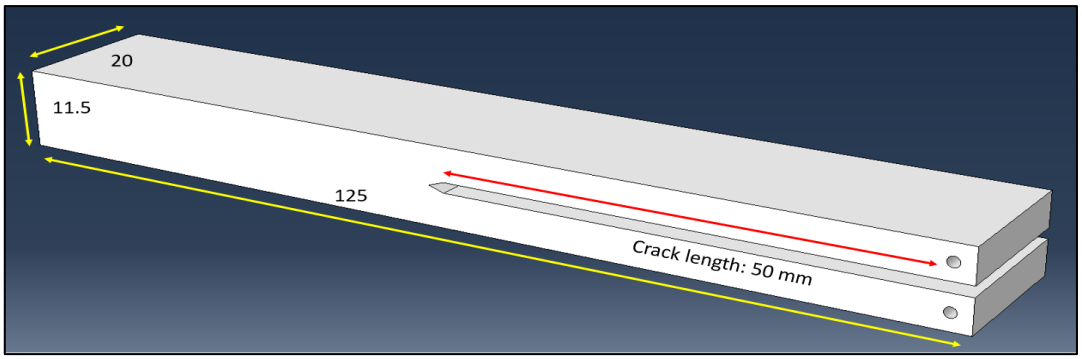

Figure 14: DCB Specimen as per ASTM D5528

The geometry was tested on a Vice to study its behaviour and to check whether crack propagation/delamination occurs. When tested, the specimen failed at the root of one of its cantilevers as shown in Figure 15.

Figure 15: Failure of initial DCB specimen design

The notch size and crack length were further changed and after a number of iterations a notch size of 13 mm and crack length of 70 mm was finalized as in Figure 16.

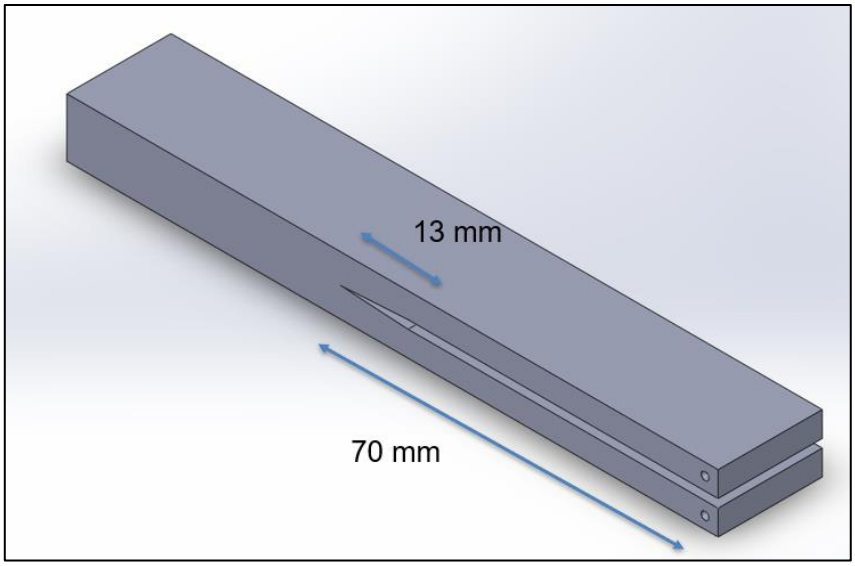

Figure 16: Final DCB specimen

The specimen model was sliced using Simplify3D. These were then printed on a Polyprinter 508 from ABS material.

Following process parameters were used:

Nozzle Temperature: 230^{o} C

Bed Temperature: 110^{o} C

Infill: 100%

Infill angle: 0^{o}

Printing Speed: 3000 mm/min

Extrusion width: Auto

Layer height: 0.2 mm

Perimeter Shells: 0

Generate Supports: On

3.2.2 DCB Testing

The specimens were tested using a Shimadzu testing machine as demonstrated in Figure 17. The specimen was loaded with the help of a metal wire that passed through the loading block region of the DCB specimen and was held by the jaws of the testing machine. Displacement was gradually applied at the rate of 3 mm/min to the upper jaw while the lower jaw remained fixed and corresponding load values were recorded by the testing machine.

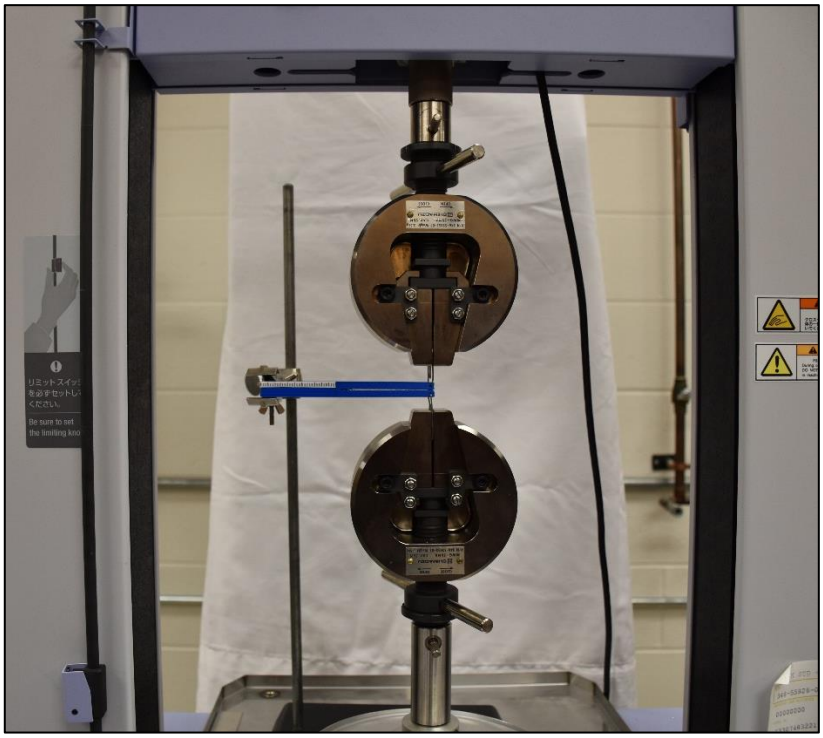

Figure 17: DCB test setup

To measure the growth in crack, a printed scale was glued on to the specimen as in Figure 18.

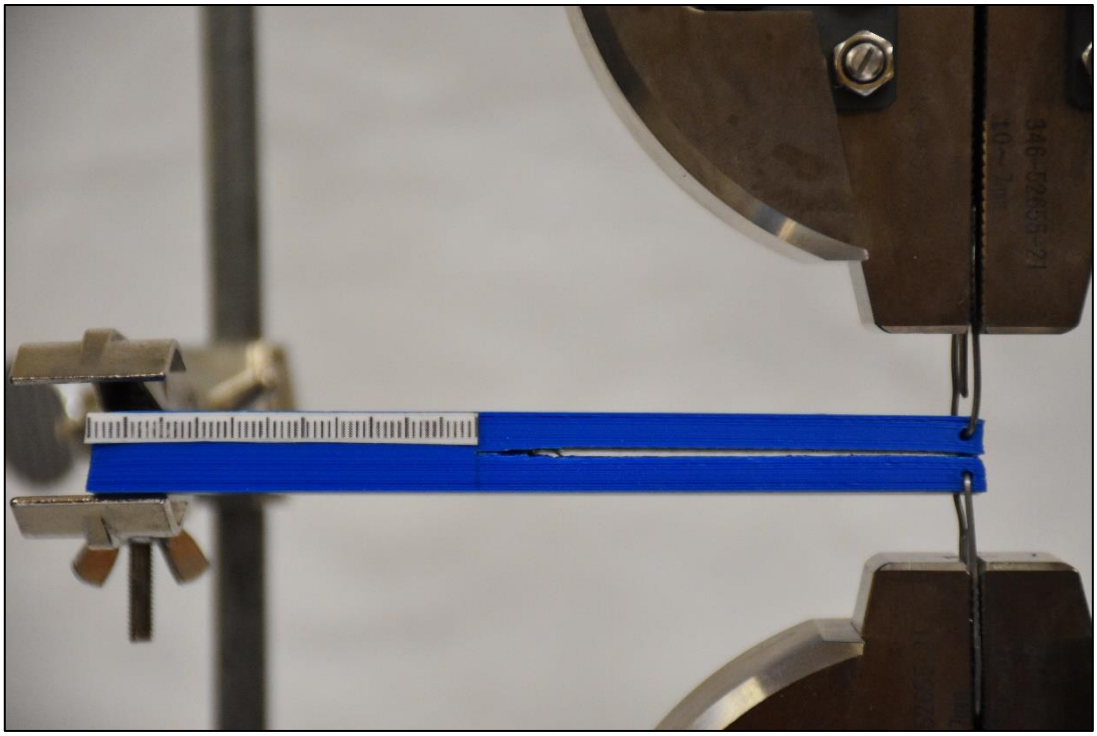

Figure 18: DCB specimen with printed scale

A video of the test was recorded. The video was analysed with a video analysis software called Tracker. In this software, the video was analysed frame by frame to relate the crack length to the corresponding values of load and displacement recorded by the testing machine.

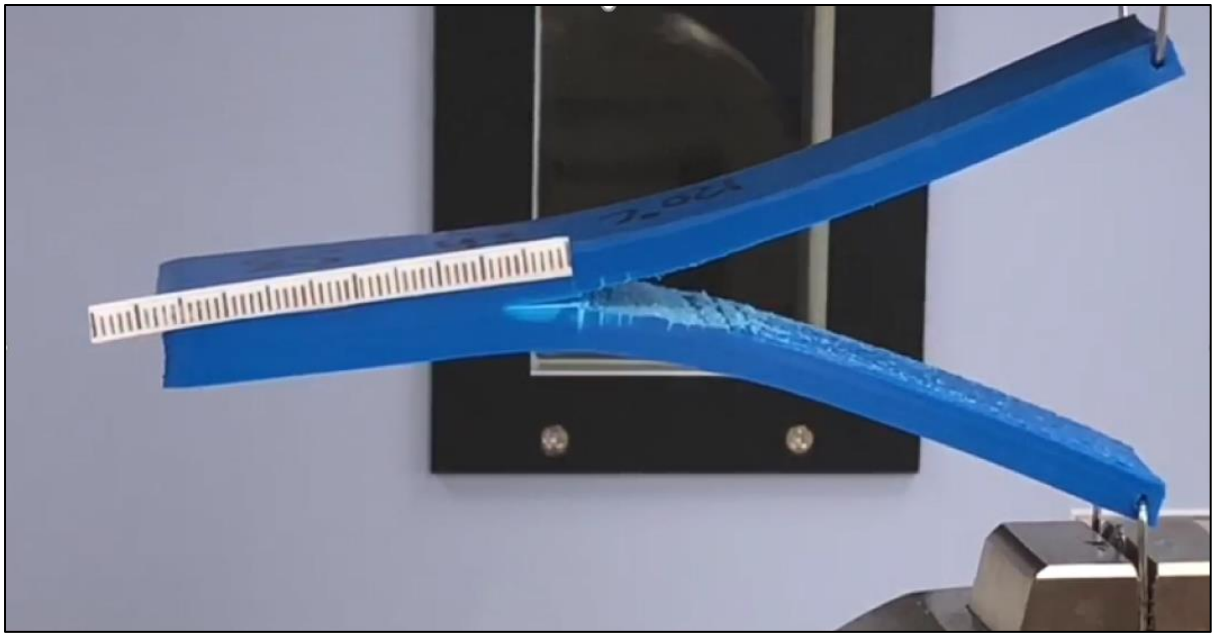

Figure 19: Crack propagation measurement

Figure 19 is a snapshot from the video showing the crack growth. The values of crack length (a), displacement (δ) and Load (P) were used to calculate the Mode I fracture toughness values (G_{IC}).

3.2.3 Meshing in Abaqus CAE

The DCB geometry was created and then meshed in Abaqus. Faces of the geometry were defined so that boundary conditions could be applied to them in BSAM. The DCB was split into two to generate an interface. An input file was generated from this mesh to be imported in BSAM.

3.2.4 Importing meshes to BSAM

The input file from Abaqus with the meshed geometry was imported in BSAM as shown in Figure 20. The DCB was split into two sections and meshed separately so as to get an interface that would delaminate.

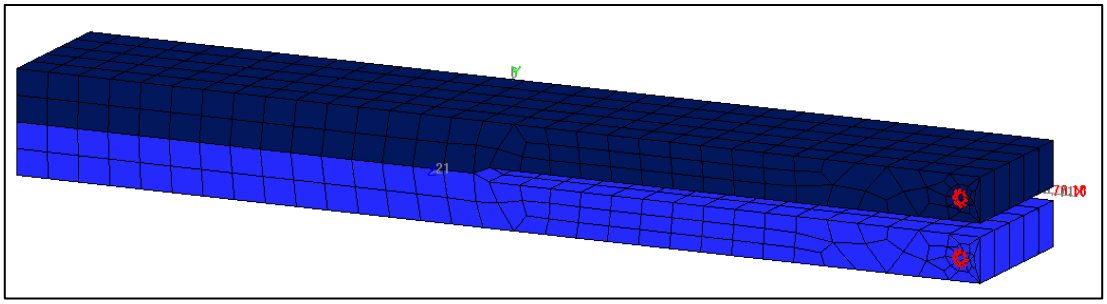

Figure 20: Meshes imported to BSAM

Interface properties are applied to this interface in the material file. This is where the obtained G_{IC} values are entered.

3.2.5 BSAM Analysis

Displacement boundary condition is applied in BSAM similar to the test method. The BSAM analysis generates force, stress, strain and delamination plots at each load step. Figure 21 and Figure 22 show the displacement and delamination plot respectively.

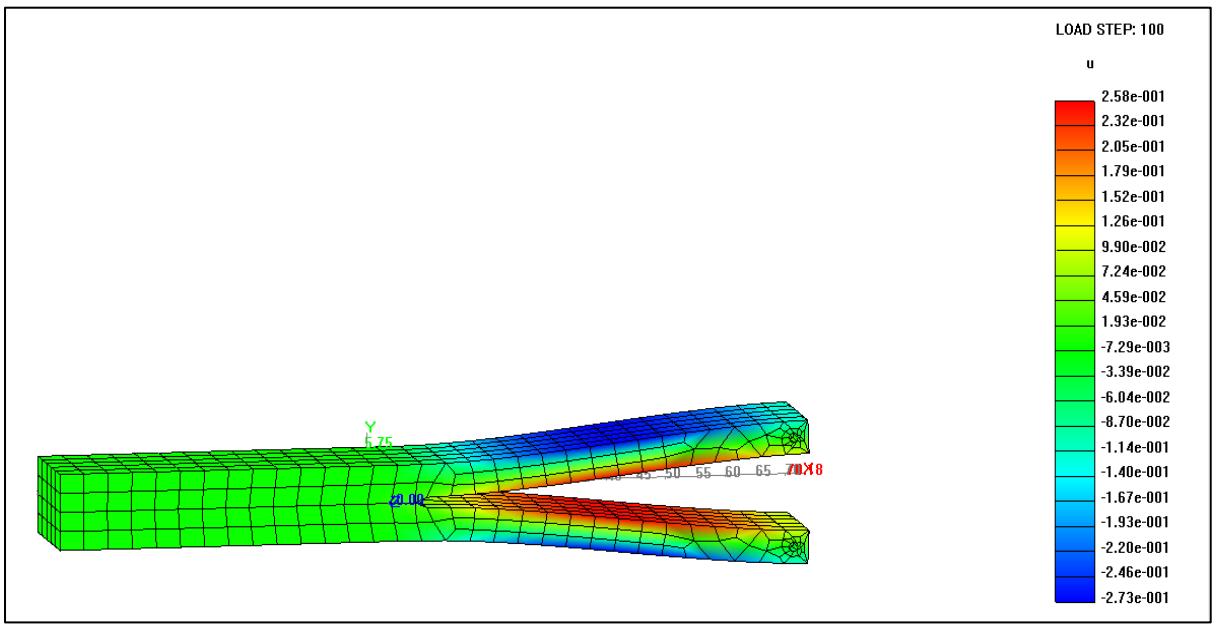

Figure 21: DCB displacement plot

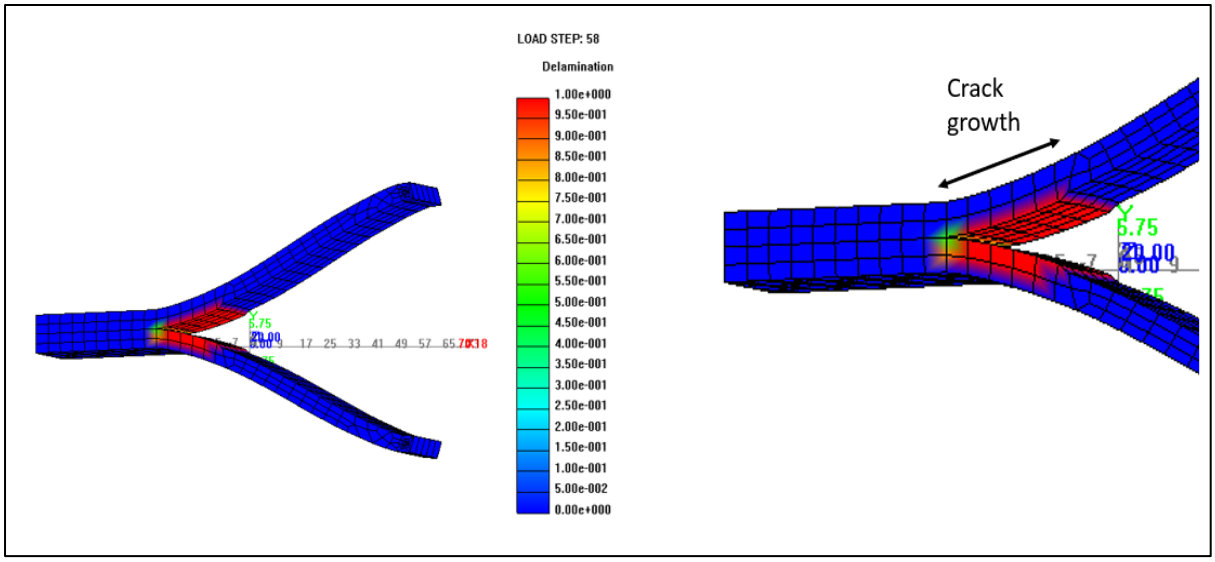

Figure 22: DCB delamination plot

3.2.6 ABS Tensile Testing

Tensile tests were carried out on ABS specimens according to ASTM D638 to calculate the Modulus values for FDM printed 90^{o} ABS specimens. The modulus values that are obtained from the fracture model are compared to the experimental modulus values to validate the fracture model. Figure 23 is a plot of the force vs displacement values from the ABS tensile test.

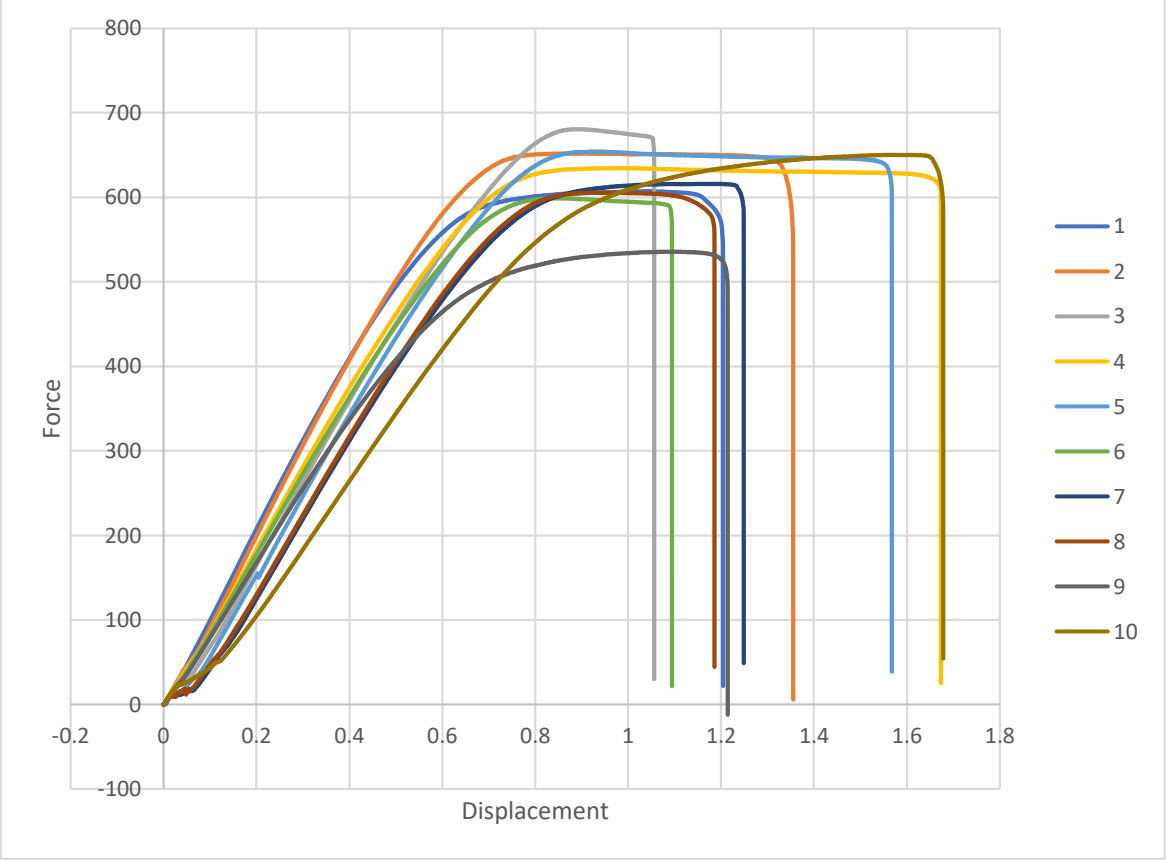

Figure 23 : Force vs Displacement graph for ABS tensile test

3.2.7 Study of Effect of temperature and heating time

3.2.7.1 Heating Fixture design and manufacturing

To study the effect of temperature and heating time on the Mode I fracture toughness values (G_{IC}), a heating fixture was required. Heating the specimens directly in an oven resulted in warpage and deformation. A heat treatment fixture to accommodate three DCB specimens at a time was designed in SolidWorks as shown in Figure 24. The blue rectangular pieces represent the DCB specimens, the orange pieces represent the spacers and the grey pieces are the end plates.

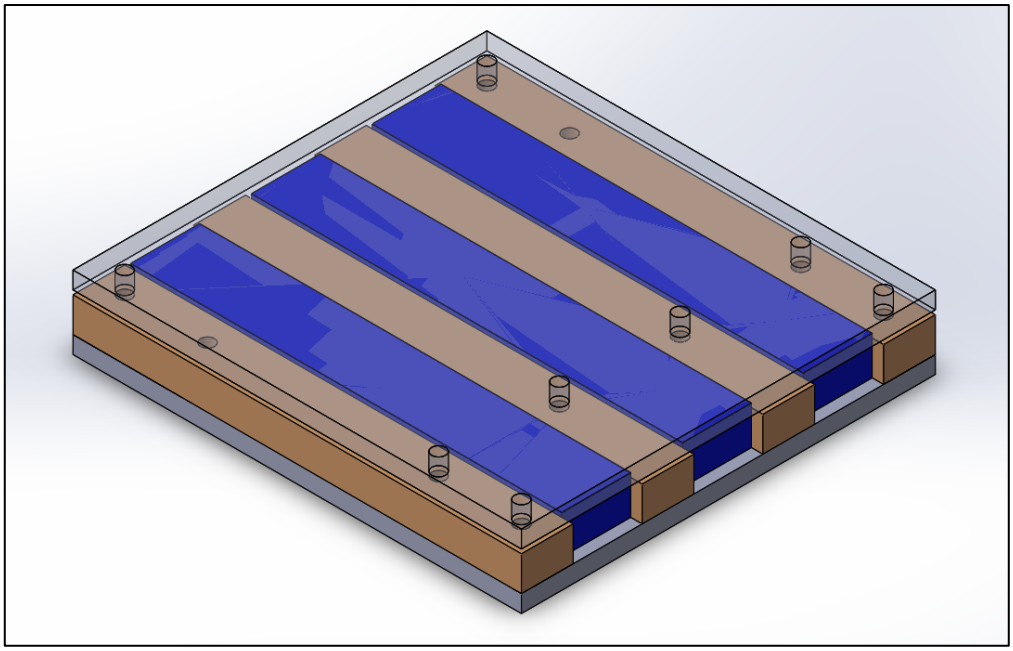

Figure 24: Heating Fixture design in SolidWorks

The plates and spacers were made of Aluminum. They were secured using screws. The final fixture is shown in Figure 25.

Figure 25: Heat treatment fixture

Specimens were heated at three temperatures - 120^{o} C, 140^{o} C and 160^{o}C for a period of 1 and 2 hours.

3.2.7.2 Heat Treatment Specimen Re-design

Due to heat treatment, the specimen grew stronger along the crack propagation direction and hence crack propagation was not observed. Instead, the specimen failed in a perpendicular direction at the root of the cantilever, as seen in Figure 26. Hence, specimen redesign was necessary.

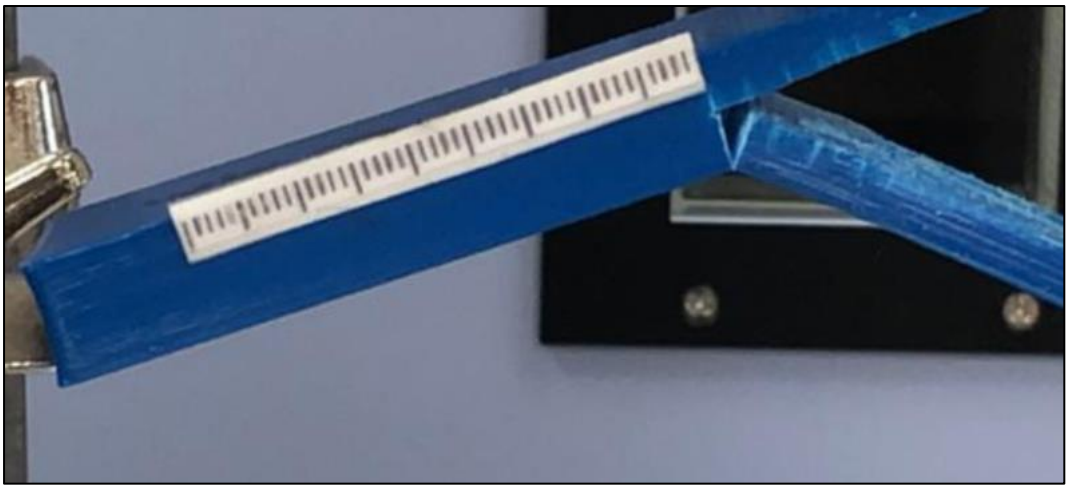

Figure 26: Heat treated specimen failing at root

After a few iterations, the new specimen was finalized and tested as shown in Figure 27

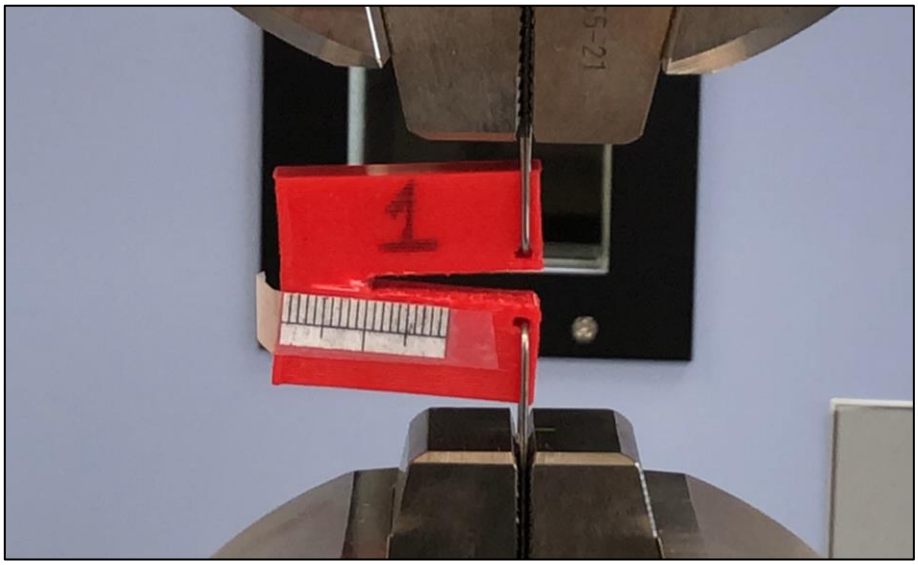

Figure 27: Redesigned heat treatment specimen

3.2.7.3 Heat treated specimen testing

The new heat treatment specimens were heated in the fixture to three temperatures - 120^{o} C, 140^{o} C and 160^{o}C. At each temperature, three specimens were kept for a period of 1 and 2 hours. This formed the basis of the following 21 tests:

Table 1: Heat Treatment tests

Test #	**Temperature**	**Time**
1	No Heat	N/A
2	No Heat	N/A
3	No Heat	N/A
4	120^{o} C	1 hr
5	120^{o} C	1 hr
6	120^{o} C	1 hr
7	140^{o} C	1 hr
8	140^{o} C	1 hr
9	140^{o} C	1 hr
10	160^{o} C	1 hr
11	160^{o} C	1 hr
12	160^{o} C	1 hr
13	120^{o} C	2 hr

14	120^{o} C	2 hr
15	120^{o} C	2 hr
16	140^{o} C	2 hr
17	140^{o} C	2 hr
18	140^{o} C	2 hr
19	160^{o} C	2 hr
20	160^{o} C	2 hr
21	160^{o} C	2 hr

Chapter 4: Results

4.1 Material Characterization

This section discusses the results obtained for the Material Characterization process. The displacement and Stiffness plots were obtained from BSAM Analysis and compared to experimental test data.

4.1.1 Displacement

The FEA analysis was run on BSAM. Displacement was applied in steps of 1% of total displacement. So, at each step, a displacement of 0.001 mm was applied. The displacement plot was generated. Figure 28 shows the displacement plot at the 10th load step for the 0^o orientation. Here, the displacement value at the load end is 0.01 mm.

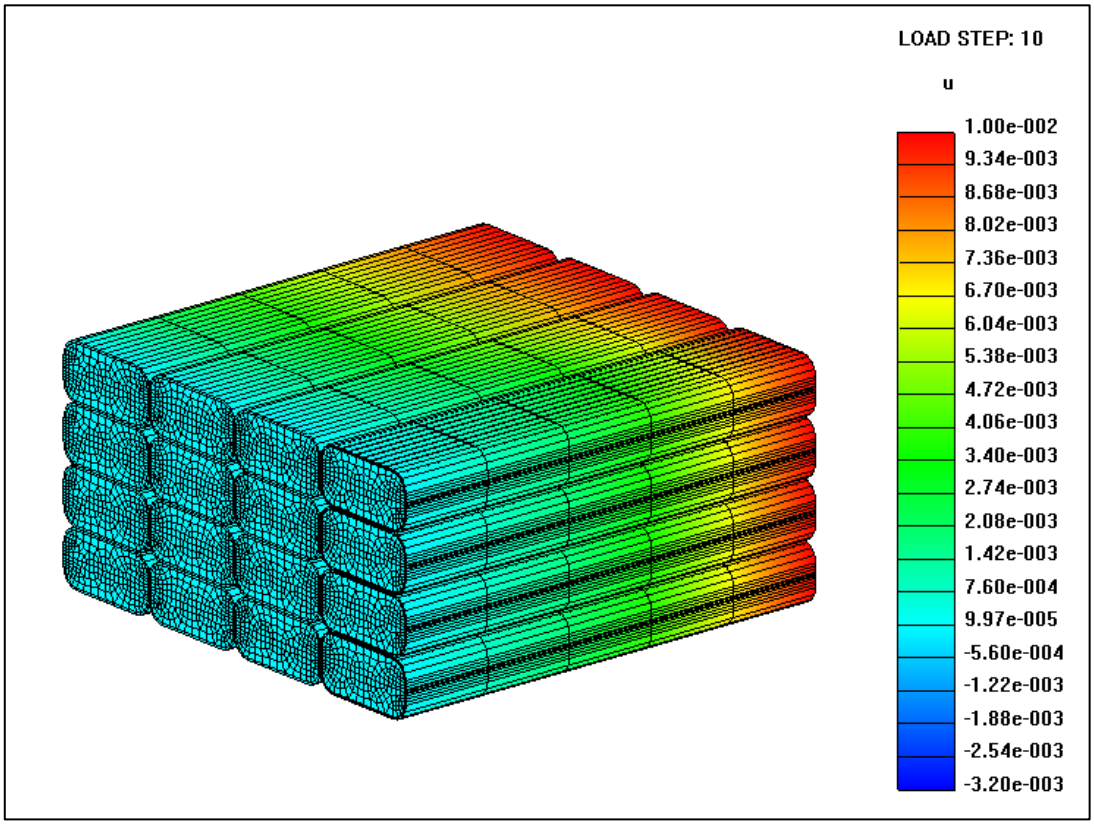

Figure 28: 0^o Displacement plot at 10th load step

Figure 29 shows the displacement plot at the 20th load step for the 30^{o} orientation. Here, the displacement value at the load end is 0.02 mm

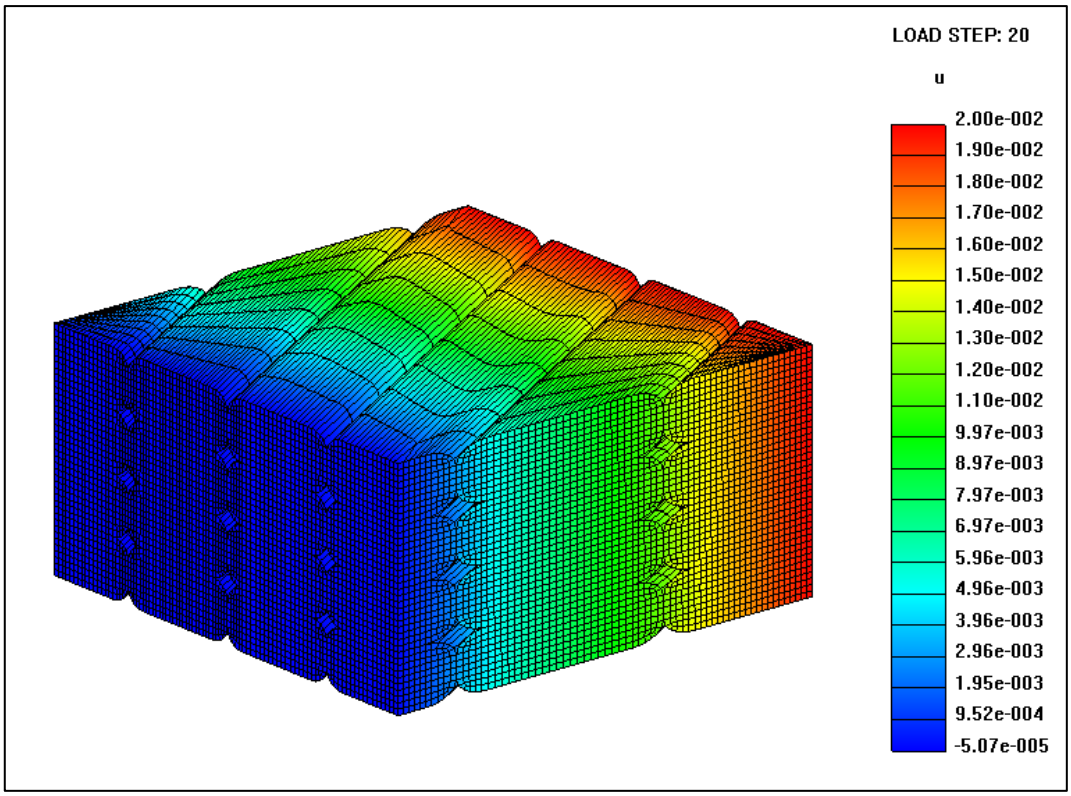

Figure 29: 30^{o} Displacement plot at 20th load step

4.1.2 Stiffness

On observing the stress distribution near the voids in Figure 30, peak stresses at the stress concentrations were within the linear range of the material. Hence, the material was considered to be a linear elastic material.

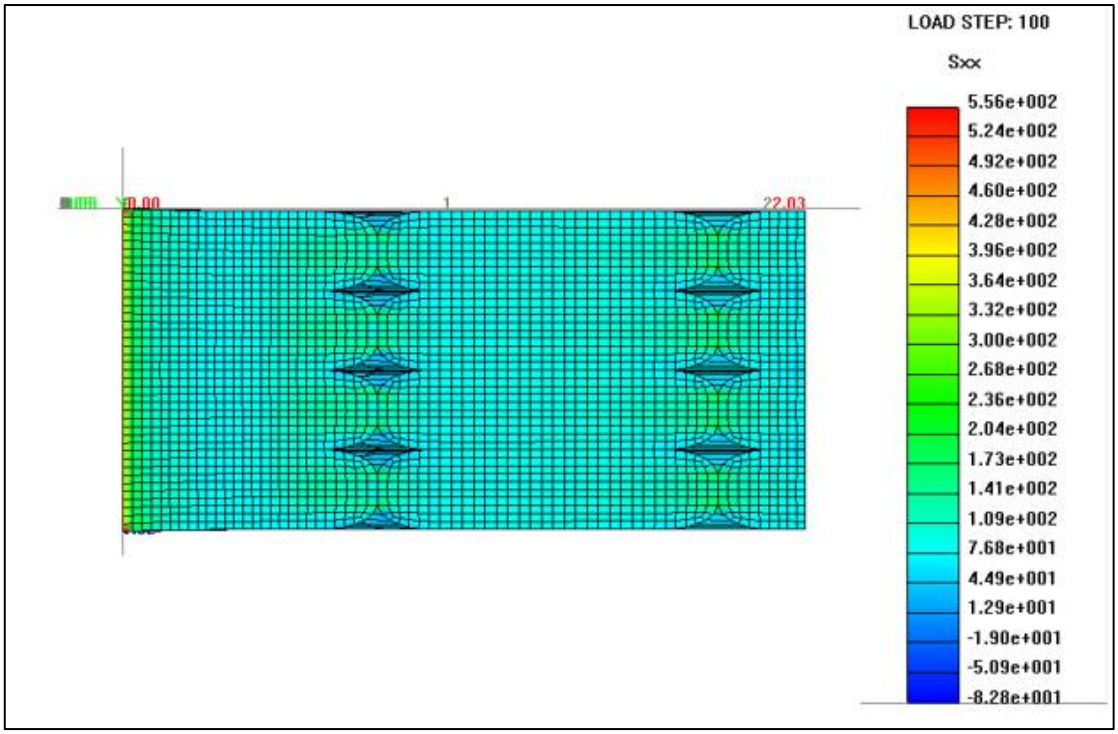

Figure 30: Stress distribution near voids

Stiffness values for different raster orientations were calculated and compared to values obtained from the experimental test data [2]. Table 2 lists the BSAM and Experimental values. As observed in Table 2, the stiffness values decrease from 0^o to 45^o raster orientations and then increase from 45^o to 90^o orientations [38].

Table 2: Stiffness Values

Raster Orientation (Degree)	**BSAM Calculated Modulus (MPa)**	**Modulus from Test Data (MPa)[1]**
0	2334.14	2369.64
15	2281.33	2277.83
30	2264.41	2161.90
45	2230.35	2046.10

[1] Calculated as average of number of specimens per raster orientation

90	2302.51	2212.14

4.1.3 Stiffness Comparison

Modulus values were calculated by tensile tests performed by Khatri on two sets of tensile specimens with different raster orientations [2]. These experimental values were compared with values obtained from BSAM. As observed in Figure 31, the stiffness values decrease from 0^o to 45^o raster orientations and then increase from 45^o to 90^o orientations. The experimental values show a similar trend as the values obtained numerically [38].

As observed in Figure 31, the BSAM modulus values obtained for raster orientations 30^o and 45^o are higher than the experimental values. Such variations could be a result of non-linearity, stress concentration, varying local geometry and machine settings. The current work models the specimens in as designed condition. To capture the variations, there is a need to model the specimens in as-built condition. The local geometry could be viewed using CT scan technology and accordingly an as-built model could be generated.

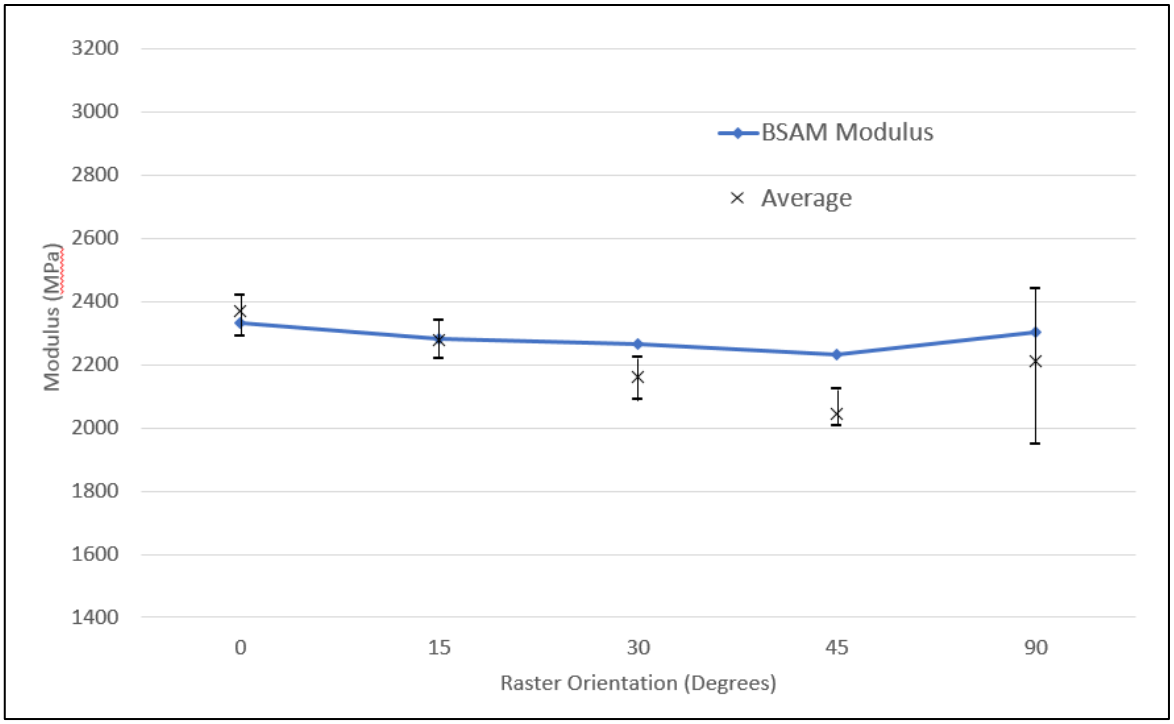

Figure 31: Comparison of Experimental and BSAM calculated Modulus Values

4.2 Fracture Predcition

4.2.1 Fracture Toughness Calculation

According to ASTM D5528, Mode I fracture toughness value (GIC) is calculated by the following formula:

$$G_{Ic} = \frac{3P\delta}{2ba}$$

Here, P is the load, δ is the load point deflection, b is the specimen width and a is the delamination length as shown in Figure 32 [37].

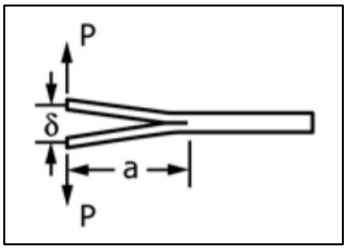

Figure 32: Notations for DCB test by ASTM D5528

The test was performed on 3 specimens and the fracture toughness value was calculated for FDM printed ABS material. Table 3 shows the data for one of the tests and the calculated G_{IC} values.

Table 3: Calculation of G_{IC} values for ABS

Force (P)	Displacement (δ)	Delamination (a)	G_{IC}
N	mm	mm	KJ/m^2
64.4358	37.37283	71	2.543819
64.07738	38.04037	72	2.539091
63.39391	38.6973	73	2.520383
59.98691	39.31237	74	2.390096
57.71239	39.66687	75	2.28927
57.28483	40.80393	76	2.30669
58.345	43.27487	77	2.459291
57.32457	44.84937	78	2.472087
56.45752	45.7359	79	2.451394

4.2.2 Heat Treated Specimen cross section

The heat-treated specimens were observed under a microscope to investigate the cross section. With no heat treatment, the cross section appears to have considerable gaps/voids between adjacent beads of the raster pattern as seen in Figure 33.

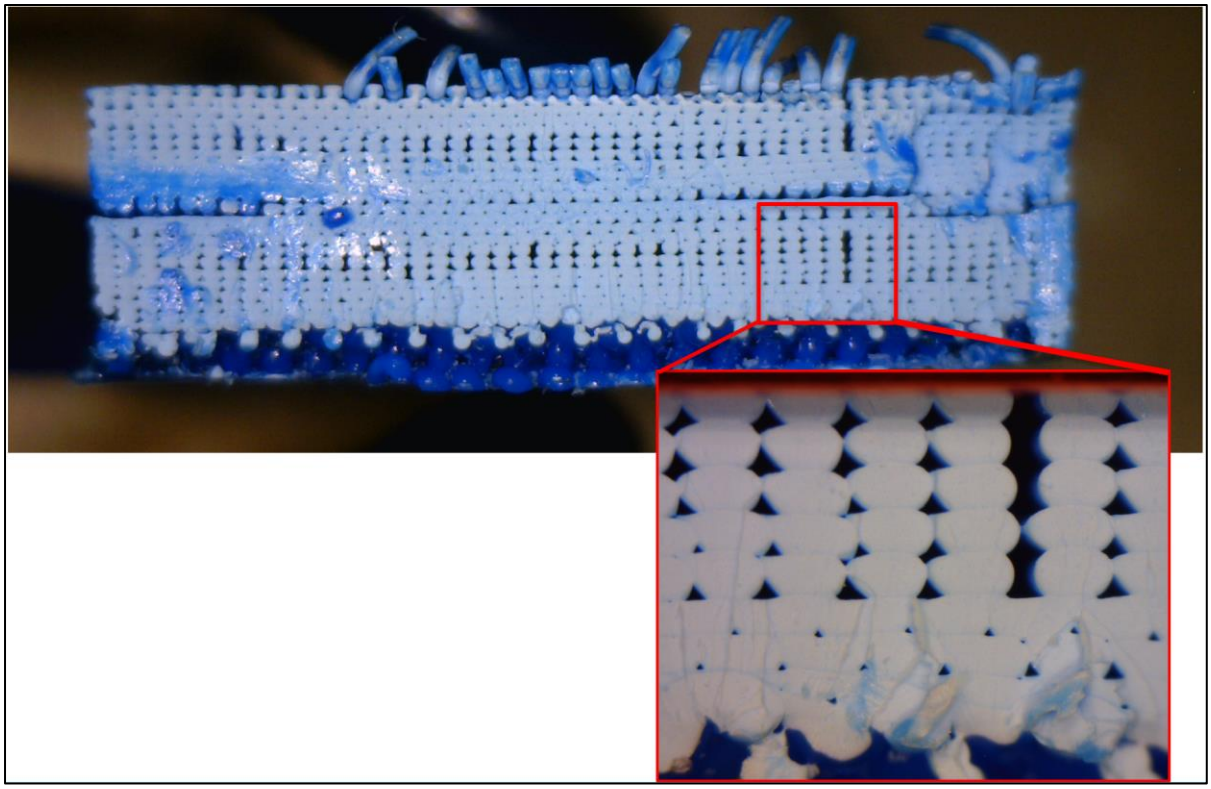

Figure 33: Specimen cross-section with no heat-treatment

When the specimen is heated in an oven to 120^{o} C, the voids appear to decrease in size as seen in Figure 34.

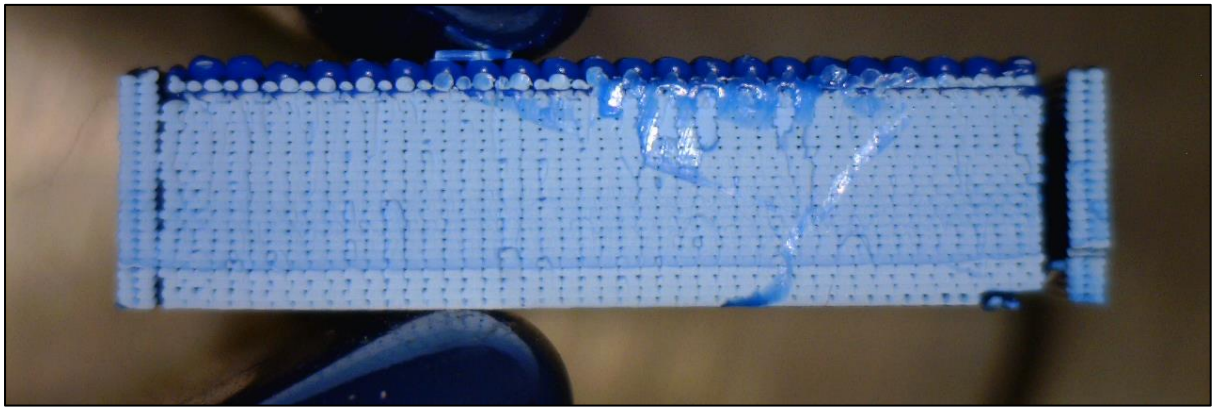

Figure 34: Specimen cross-section heated at 120^{o} C

At 140^{o} C, the voids continue to decrease in size with few layers completely merging together as observed in Figure 35. This is more prominent near the top and bottom layers that are in direct contact with the Aluminium fixture surface.

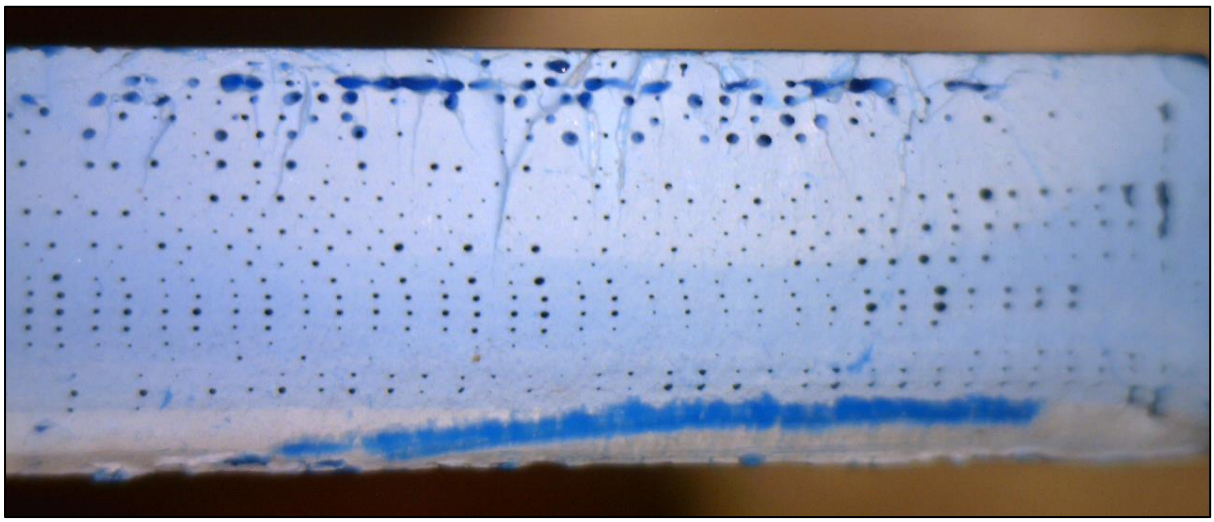

Figure 35: Specimen cross-section heated at 140^{o} C

At 160^{o} C, the voids disappear or are negligible as observed in Figure 36. Adjacent layers completely fuse to each other creating a cross-section similar to a solid specimen. The 3D printed layered structure is no longer visible.

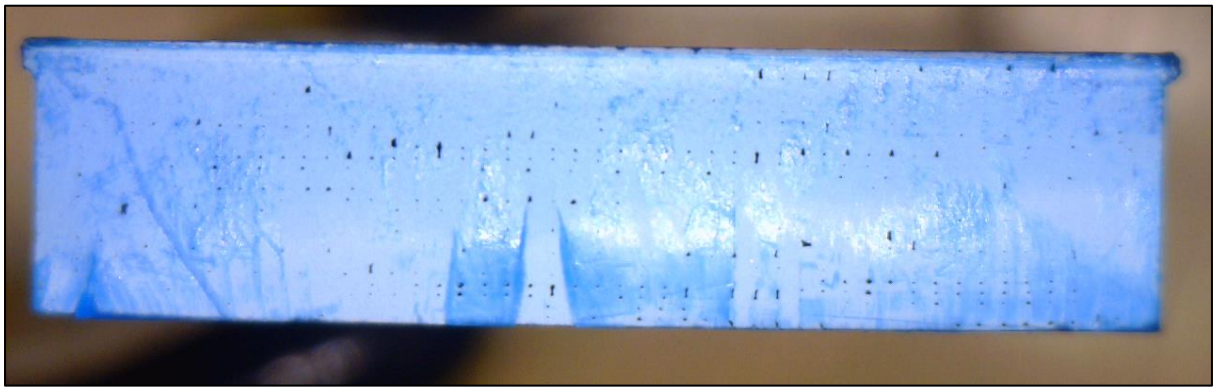

Figure 36: Specimen cross-section heated at 160^{o} C

Force vs Stroke values were plotted for the 21 tests. Following were the observations:

4.2.3 Temperature Effect, keeping heating time constant at 1hr

As temperature increased from 120^{o} C to 160^{o} C, the strength increased as seen in Figure 37

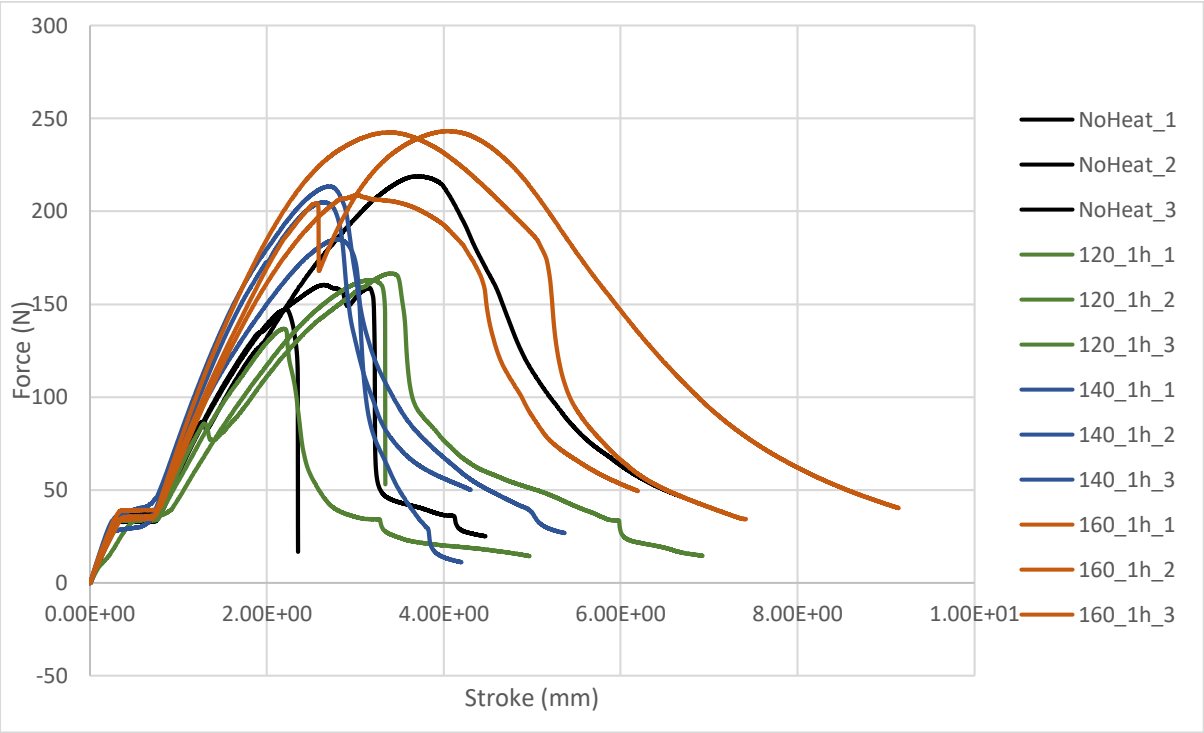

Figure 37: Effect of Temperature at 1 hr

4.2.4 Temperature Effect, keeping heating time constant at 2hr

When heating time was increased to 2 hrs, the strength increased when the temperature was increased from 120^{o} C to 140^{o} C but there was no significant increase when the temperature was further increased to 160^{o} C. This can be observed in Figure 38.

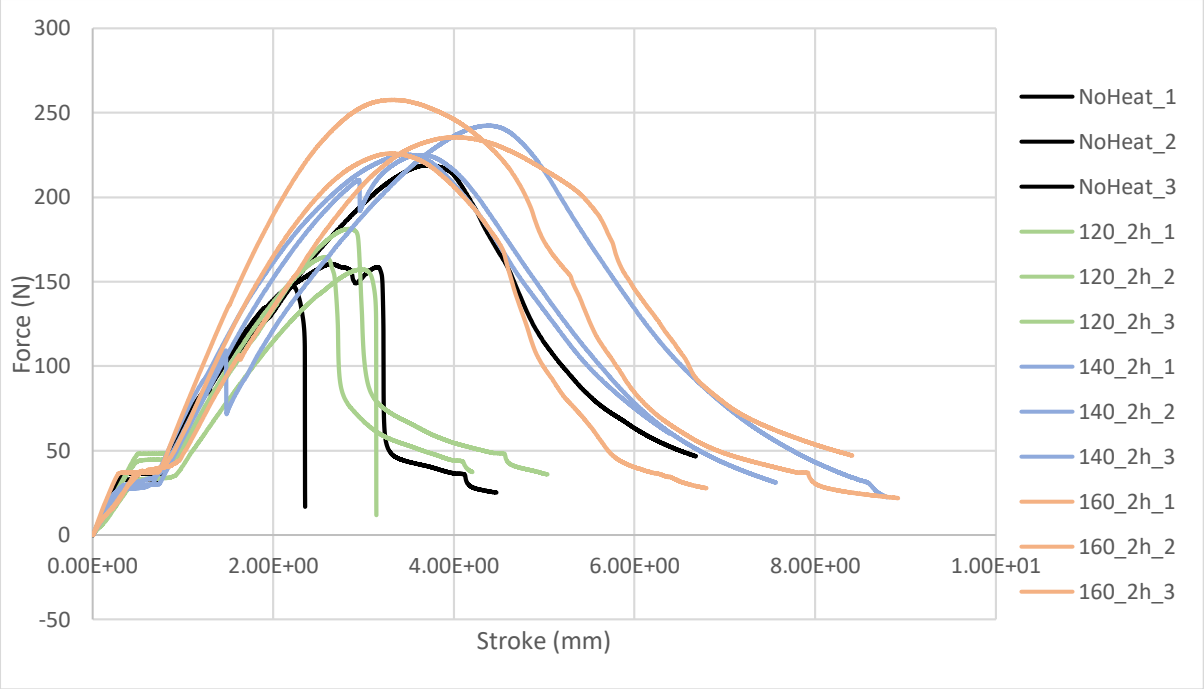

Figure 38: Effect of Temperature at 2 hrs

4.2.5 Effect of heating time, keeping temperature constant at 120^{o} C

When the heating time was increased from 1 hr to 2 hrs, an increase in strength was observed as seen in Figure 39 . However, this increase in small (10N -20N) compared to the increase at 140^{o} C (~50N).

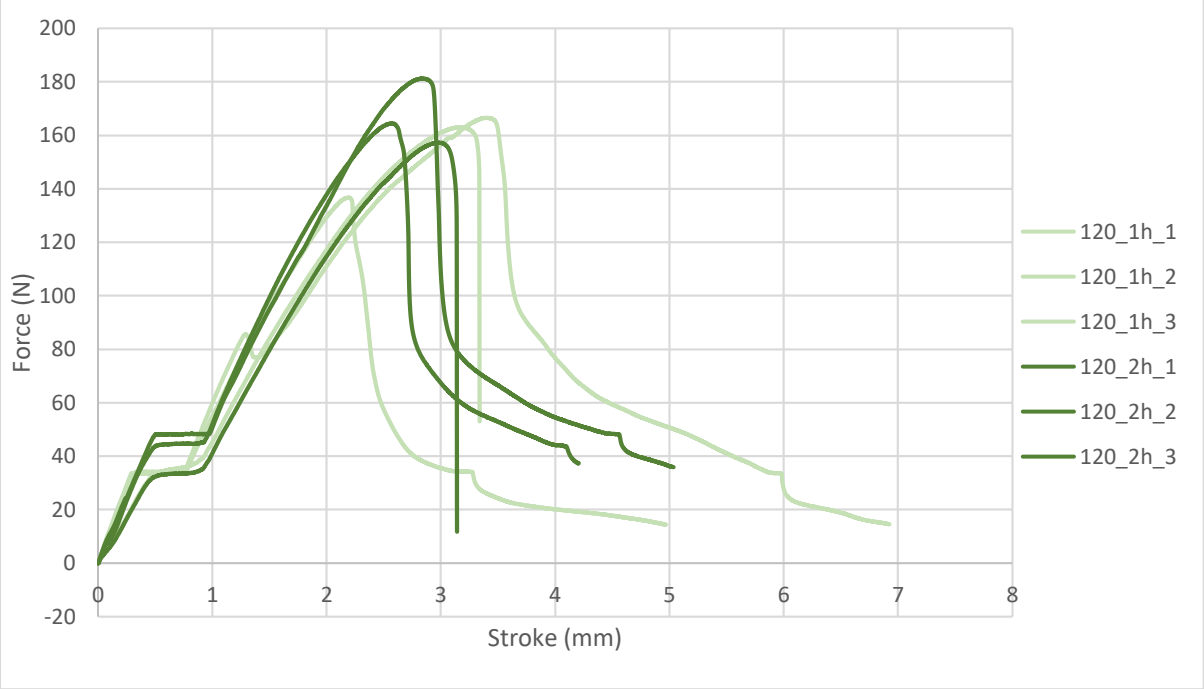

Figure 39: Effect of heating time at 120^{o} C

4.2.6 Effect of heating time, keeping temperature constant at 140^{o} C

At 140^{o} C, the strength increased by about 50 N as observed in Figure 40

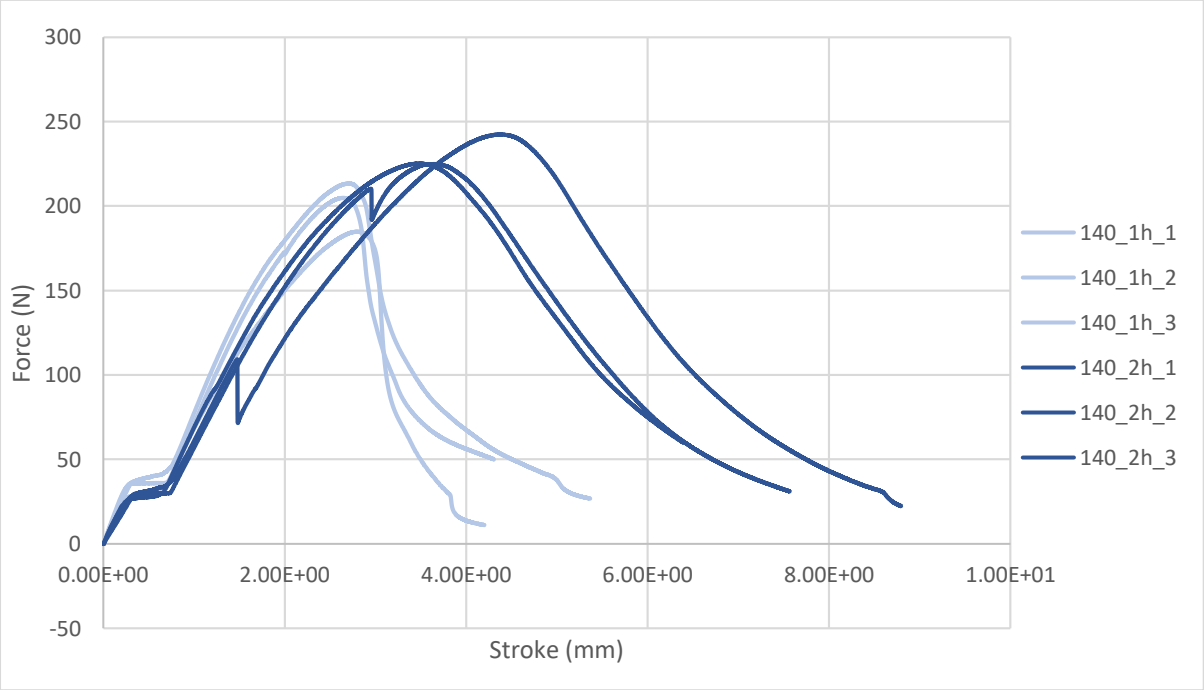

Figure 40: Effect of heating time at 140^{o} C

4.2.7 Effect of heating time, keeping temperature constant at 160^{o} C

At 160^{o} C, heating time had negligible effect on the strength as observed in Figure 41.

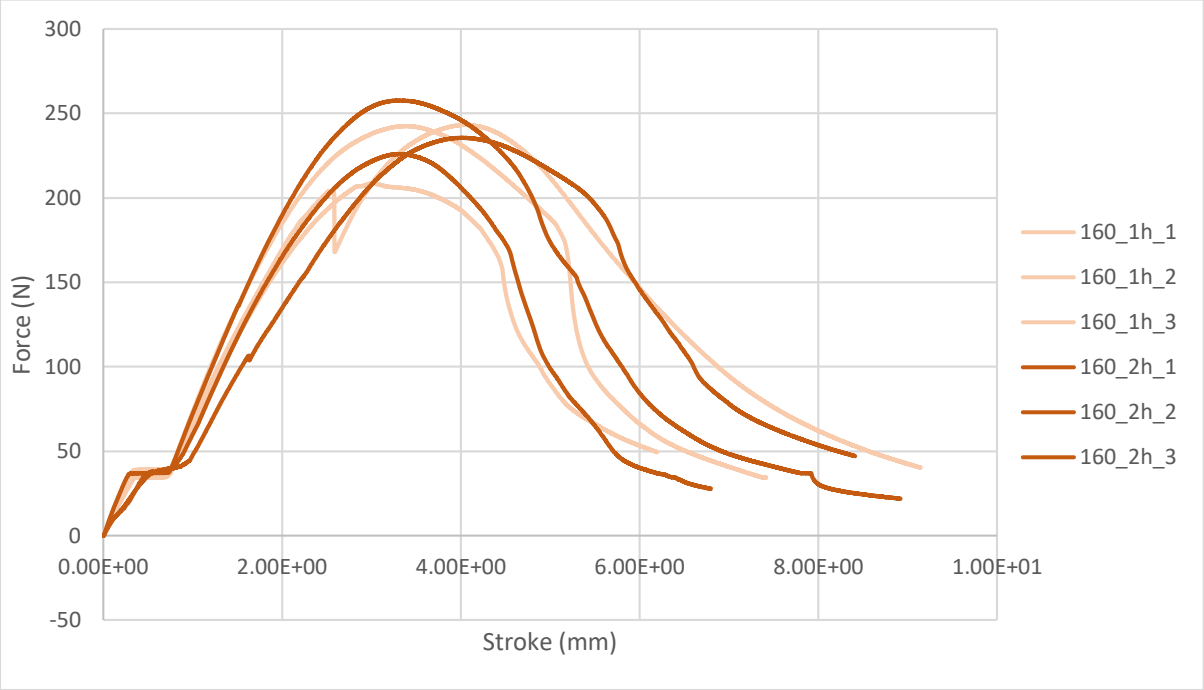

Figure 41: Effect of heating time at 160^{o} C

4.2.8 Crack growth measurement challenges

The tests on the heat-treated specimens were recorded using a normal phone camera that has a frame rate of 60 fps. Since the length of the specimen was small, the time between crack initiation and complete delamination was short. Hence, it was challenging to accurately measure the crack growth as well as note the force and displacement readings. To overcome this, a camera with a high frame rate (~240 fps) should be used along with Tracker, a video analysis and modeling software to accurately measure the crack growth with respect to force and displacement.

Chapter 5: Conclusion

5.1 Material Characterization

Section A of this work presents a procedure for numerically predicting the Elastic Modulus of FDM printed parts as a function of raster angle. In this work, 0, 15, 30, 45, 90-degree FDM raster orientations were modelled and meshed using ABAQUS and the Elastic Modulus values for these orientations were numerically predicted using BSAM. These modulus values were observed to decrease from 0^o to 45^o and then increase from 45^o to 90^o. These values show a similar trend when compared to experimental testing data [38].

5.2 Fracture Prediction

Section B of this work demonstrates a procedure for developing a model for numerically predicting delamination and eventually fracture in FDM printed parts. Fracture toughness (G_{IC}) values were calculated by testing ABS DCB specimens. These values can be used to develop the BSAM model that can predict delamination/fracture. Further in this section, the effect of temperature and time of heating on the strength of the DCB specimen is studied. Observing the cross-sections for specimens at room temperature, 120^o C, 140^o C and 160^o C reveals that the specimens initially contain a large number of gaps/voids which reduce in size as the temperature is increased and almost vanish at 160^o C. For a heating time of 1 hour, the strength was observed to increase as the temperature was increased from 120^o C to 140^o C and then to 160^o C. For a heating time of 2 hours, there was considerable increase in strength when the temperature was increased from 120^o C to 140^o C. But the increase was negligible when the temperature was increased to 160^o C. When studying the effect of heating time on the strength of the specimens, there was about 20N increase in strength when the time was increased from 1hr to 2hr for the specimen at 120^o C. At 140^o C, this increase was about 50N

and at 160^{o} C there was no change in the strength. From these observations, we can conclude that the cross-section becomes dense with increase in temperature which increases the strength of the specimen. With time, the increase in strength of the specimen is considerable at lower temperatures but is negligible at higher temperatures.

Chapter 6: Future Work

6.1 Optimizing Goemetry of the DCB specimens & measuring crack growth

Since the length of the current DCB was small, crack propagation was fast over a short length. This could not be captured with a normal camera. A camera with a high FPS can be used to measure this crack length or the DCB geometry can be optimized further to observe considerable crack propagation in order to calculate the G_{IC} values.

6.2 Optimizing the BSAM model with obtained stiffness and G_{IC} values

The stiffness values from tensile testing and fracture toughness values from DCB testing can be used to develop the BSAM model that can be used to predict delamination.

6.3 Study the effect of temperature and time on G_{IC} values

The effect of temperature on the G_{IC} values can be studied by heating the DCB specimens to different temperatures for different periods of time.

6.4 Study the effect of pressure

The effect of pressure on the strength of the heat-treated specimens can be studied and corresponding G_{IC} values can be determined.

References

[1] ASTM ISO/ASTM52900-15 Standard Terminology for Additive Manufacturing — General Principles — Terminology, ASTM International, 2015.

[2] Khatri, Amit. Effect of Manufacturing-Induced Defects and Orientation on the Failure and Fracture Mechanism of 3d Printed Structures, Master's Thesis, University of Texas at Arlington, 2016.

[3] T. Osborn, E. Zhou, R. Gerseski, D. Mollenhauer, G.P. Tandon, T.J. Whitney, and E.V. Iarve, "Experimental and Theoretical Evaluation of Stiffness Properties of Fused Deposition Modeling Parts," American Society of Composites-30th Technical Conference. 2015.

[4] Scopigno R., Cignoni P., Pietroni N., Callieri M., Dellepiane M. (2017). "Digital Fabrication Techniques for Cultural Heritage: A Survey". Computer Graphics Forum 36 (1): 6–21. DOI:10.1111/cgf.12781

[5] ASTM Standard D638 - 10. (2010). Standard Test Method for Tensile Properties of Plastics. ASTM International, West Conshohocken, Pennsylvania, DOI: 10.1520/D0638-10.

[6] S. H. Ahn, M. Montero, D. Odell, S. Roundy, P. K. Wright, "Anisotropic Material Properties of Fused Deposition Modeling ABS", Rapid Prototyping, 8(4) (2002) 248-257.

[7] Bellini, Anna, and Selçuk Güçeri. "Mechanical Characterization of Parts Fabricated Using Fused Deposition Modeling." Rapid Prototyping Journal 9.4 (2003): 252-264.

[8] Jaret Riddick, Asha Hall, Mulugeta Haile, Ray Von Wahlde, Daniel Cole, and Stephen Biggs, "Effect of Manufacturing Parameters on Failure in Acrylonitrile-butadiane-styrene Fabricated by Fused Deposition Modeling." Proceedings of the 53rd

AIAA/ASME/ASCE/AHS/ASC Structures, Structural Dynamics and Materials Conference, Honolulu, HI, 2012.

[9] Ziemian, Constance, Mala Sharma, and Sophia Ziemian. "Anisotropic Mechanical Properties of ABS Parts Fabricated by Fused Deposition Modelling." in Mechanical Engineering, Murat Gokcek (Ed.), InTech, 2012.

[10] Ziemian, Sophia, Maryvivian Okwara, and Constance Wilkens Ziemian. "Tensile and Fatigue Behavior of Layered Acrylonitrile Butadiene Styrene." Rapid Prototyping Journal 21.3 (2015): 270-278.

[11] Lee, John, and Adam Huang. "Fatigue Analysis of FDM Materials." Rapid Prototyping Journal 19.4 (2013): 291-299.

[12] Afrose, M. F., Masood, S. H., Iovenitti, P., Nikzad, M., & Sbarski, I. "Effects of Part Build Orientations on Fatigue Behaviour of FDM-processed PLA Material." Progress in Additive Manufacturing 1.1-2 (2016): 21-28.

[13] Zhang, Hanyin. Characterization of Tensile, Creep, and Fatigue Properties of 3D Printed Acrylonitrile Butadiene Styrene. Master's Thesis, Purdue University Indianapolis. 2016.

[14] Motaparti, Krishna Prasanth. Effect of Build Parameters on Mechanical Properties of Ultem 9085 Parts by Fused Deposition Modeling. Master's Thesis, Missouri University of Science and Technology, 2016.

[15] Torrado, Angel R., and David A. Roberson. "Failure Analysis and Anisotropy Evaluation of 3D-printed Tensile Test Specimens of Different Geometries and Print Raster Patterns." Journal of Failure Analysis and Prevention 16.1 (2016): 154-164.

[16] Huang, Bin, and Sarat Singamneni. "Raster Angle Mechanics in Fused Deposition Modelling." Journal of Composite Materials 49.3 (2015): 363-383.

[17] Rezayat, H., Zhou, W., Siriruk, A., Penumadu, D., & Babu, S. S. "Structure–mechanical Property Relationship in Fused Deposition Modelling." Materials Science and Technology 31.8 (2015): 895-903.

[18] Ravi Patel, H.N.Shah, Susheela V. Kumari, “Experimental Investigation of Fracture of ABS Material by ASTM D-5045 for Different Crack Length & Layer of Orientation Using FDM Process,” International Journal of Mechanical and Industrial Technology, Vol. 3, Issue 1, (2015):79-83.

[19] Ulu, Erva, et al. "Enhancing the Structural Performance of Additively Manufactured Objects Through Build Orientation Optimization." Journal of Mechanical Design 137.11 (2015): 111410.

[20] Torres, Jonathan, Jonathan Torres, Matthew Cole, Matthew Cole, Allen Owji, Allen Owji, Zachary DeMastry, Zachary DeMastry, Ali P. Gordon, and Ali P. Gordon, "An approach for mechanical property optimization of fused deposition modeling with polylactic acid via design of experiments." Rapid Prototyping Journal 22.2 (2016): 387-404.

[21] El-Gizawy, A. Sherif, Shan Corl, and Brian Graybill. "Process-induced Properties of FDM Products." Proceedings of the ICMET, International Conference on Mechanical Engineerings and Technology Congress & Exposition. 2011.

[22] Li, Longmei, Qiao Sun, Celine Bellehumeur, and Peihua Gu. "Composite Modeling and Analysis for Fabrication of FDM Prototypes with Locally Controlled Properties." Journal of Manufacturing Processes 4.2 (2002): 129-141.

[23] Sayre III, Robert. A Comparative Finite Element Stress Analysis of Isotropic and Fusion Deposited 3D Printed Polymer. Master’s Thesis, Rensselaer Polytechnic Institute Hartford, (2014).

[24] Rodríguez, José F., James P. Thomas, and John E. Renaud. "Mechanical Behavior of Acrylonitrile Butadiene Styrene Fused Deposition Materials Modeling." Rapid Prototyping Journal 9.4 (2003): 219-230.

[25] Park, Sang-in, and David W. Rosen. "Quantifying Mechanical Property Degradation of Cellular Material Using As-fabricated Voxel Modeling for the Material Extrusion Process." Proceedings of the Annual Solid Freeform Fabrication Symposium, Austin. 2015.

[26] Baikerikar, Prathamesh. Comparison of As-built FEA Simulations and Experimental Results for Additively Manufactured Dogbone Geometries. Master's Thesis, Clemson University, (2017).

[27] Faes, Matthias, Eleonora Ferraris, and David Moens. "Influence of Inter-Layer Cooling Time on the Quasi-static Properties of ABS cComponents Produced via Fused Deposition Modelling." Procedia CIRP 42 (2016): 748-753.

[28] Hoos K, Swindeman M, Whitney T, et al. "B-spline analysis method (BSAM)-FE, user manual," University of Dayton Research Institute, March 2014.

[29] Iarve, E. V., "Mesh independent modelling of cracks by using higher order shape functions," International Journal of Numerical Methods in Engineering, (2003)

[30] Iarve, E. V., Gurvich, M. R., Mollenhauer, D. H., Rose, C. A. and Dávila, C. G., "Mesh-independent matrix cracking and delamination modeling in laminated composites." International Journal of Numerical Methods in Engineering, (2011)

[31] Michael J. Swindeman, Endel V. Iarve, Robert A. Brockman, David H. Mollenhauer, and Stephen R. Hallett. "Strength Prediction in Open Hole Composite Laminates by Using Discrete Damage Modeling", American Institute of Aeronautics and Astronautics Journal, (2013)

[32] H. K. Adluru, K. H. Hoos, E. V. Iarve, “Discrete Damage Modelling of Delamination Migration in Clamped Tapered Laminated Beam Specimens”, Proceedings of the American Society for Composites—Thirty-second Technical Conference, (2017)

[33] H. K. Adluru, K. H. Hoos, E. V. Iarve, J. G. Ratcliffe, “Delamination Initiation and migration modeling in clamped tapered laminated beam specimens under static loading”, Composites Part A: Applied Science and Manufacturing.

[34] N. Moes, J. Dolbow, T. Belytschko, “ A Finite Element Method for Crack Growth without Remeshing,” International Journal of Numerical Methods in Engineering, (1999)

[35] N. V. de Carvalho, B. Y. Chen, S. T. Pinho,P. M. Baiz, T. E. Tay, “Floating node method and Virtual Crack Closure technique for Modeling Matrix Cracking- Delamination Migration,” (2013)

[36] T. D. Breitzman, R. P. Lipton and E. V. Iarve, "Local field assessment inside multiscale composite architectures," SIAM Journal on Multiscale Modeling & Simulation, vol. 6, no. 3, pp. 937-962, (2007).

[37] ASTM D5528-13 Standard Test Method for Mode I Interlaminar Fracture Toughness of Unidirectional Fiber-Reinforced Polymer Matrix Composites, ASTM International, NASA/CR-2013-218022, (2013).

[38] S. Sheth, R. M. Taylor, and H. K. Adluru, “Numerical Investigation of Stiffness Properties of FDM Parts as a Function of Raster Orientation,” Solid Freeform Fabrication 2017: Proceedings of the 28th Annual International Solid Freeform Fabrication Symposium – An Additive Manufacturing Conference, (2017).

Biographical Information

Sanchita Sheth earned her Bachelor of Engineering (B.E) degree in Mechanical Engineering from K. J. Somaiya College of Engineering, Mumbai in 2014. She worked as a Design Engineer at Godrej Appliances for two years. She joined the Mechanical Engineering department of The University of Texas at Arlington where she earned her Master of Science (M.S) degree in Mechanical Engineering in 2018.

Sanchita's interests include Product Design, Testing, Additive Manufacturing. During her master's program, she interned as a Design Engineer for two semesters at Tesla working on the Model 3 door trim components. Her research at UTA is focused on developing reliable material characterization for Additive Manufactured parts, specifically Fused Deposition Modelling (FDM). After graduating, she joined Café X Technologies as a Mechanical Design Engineer developing the hardware for a robotic coffee bar.